MULTI-HAZARD RISK ASSESSMENT ON ROAD INFRASTRUCTURES- A framework for assessing the earthquake and rain-induced landslide resilience of a road network in Turin, Italy, with multiple RC bridges and a tunnel

1. Acknowledgment

This thesis marks the completion of my master's degree at Politecnico di Torino in the field of Civil Engineering. I am deeply grateful to my supervisors. Professor Marco Civera and PhD. Fabrizio Aloschi has made a significant contribution to this work. I extend my sincere thanks for their guidance and support throughout this project. Their constant availability and valuable insights have significantly enhanced my work and motivation.

I would also like to express my gratitude to all my professors who taught during my studies at Politecnico di Torino; it has been an honor studying in their classes. I would like to thank my parents who made it possible for me to travel across the world and pursue this degree. This would not have been possible without their constant support and guidance. I would like to express my gratitude to my fiancé, who constantly pushed me to do better and motivated me. And in no order, I would just like to name some of my friends, Adiya Hasan, Usman Ashraf, Maryam Akhmedova, and Arman Hussain, all of whom have been there for me in one form or another for the last three years.

2. Abstract

In the era where unpredictable and extreme weather events are becoming increasingly frequent, it is important to have infrastructure that is resilient and can remain functional during and after a natural hazard event. A nation or a region's economy heavily relies on the smooth operation of its road network. However, road infrastructure is always vulnerable to natural hazards that can lead to anything from minor disruptions to road closures lasting several months. This master's thesis focuses specifically on calculating the efficiency index of the road network under multi-hazard conditions in the region of Piemonte, Italy. To evaluate the efficiency index, we must determine the geotechnical stability of the slope and analyze the structural stability of buildings and bridges along the RN. For this thesis, the road can be disturbed by three factors: the first is the EQIL (earthquake-induced landslide). For this, we must do a detailed study involving the modeling of slopes in the study area using QGIS and DEM data.

Various geotechnical parameters, such as effective friction angles, cohesion, and soil volumetric mass, were assigned to the registered landslides. To estimate stability, factors of safety (FS) were calculated for both dry and fully saturated conditions, followed by the determination of critical acceleration (ac). Together with the modelling, seismic data from the INGV database were used to

determine the peak ground acceleration (PGA) for calculating Newmark displacement. Two scenarios were considered: dry conditions and fully saturated conditions. The results of the stability analysis showed that slopes with an FS value less than one are inherently unstable and likely to fail without external triggers. Under fully saturated conditions, the probability of failure increased significantly. The Newmark displacement analysis provided insight into additional earthquake risks, improving the ability to predict and mitigate landslides effectively. Finally, the results of the Newmark displacement calculations for each landslide along the four roads are presented in Appendix B. Slopes with FS values below one, and thus negative ac values, are still shown in red and will not display displacement according to the calculations. However, displacement will occur before an earthquake trigger occurs, exacerbating the situation. Some landslides were marked in yellow, meaning they have a calculated DN value and are sensitive to seismic activity. Now, for the second hazard, we must study how damage caused to buildings and bridges due to a seismic event impacts the overall efficiency of the road network. To achieve this, we first needed to obtain data for all the buildings and bridges along the road network. And then calculate the PGAcap with respect to the damage state. This study is important for making roads and infrastructure safer by examining the causes of landslides and utilizing tools to assess the associated risks. The determination of the critical acceleration provides the opportunity for further analysis, such as determining road efficiency using an efficiency index. Lastly, we tried to calculate the economic impact of road disruptions on the surrounding communities and businesses.

3. Table of Contents

1. Acknowledgment 1
2. Abstract 1
3. Table of Contents 2
4. List of Acronyms 4
5. List of Tables: 4
6. List of Figures: 5
7. Introduction 6
8. Multi-Hazard Risk Assessment on Road Infrastructure. 7
9. Hazard Modeling and Risk Assessment 9
   - 9.1 Built-Up Environment Risk and Hazard Assessment 10
   - 9.2 Landslide Risk and Hazard Assessment 12
     - 9.2.1 Landslide Risk Assessment 13
   - 9.3 Earthquake-Induced Landslides: 13
   - 9.4 Risk Assessment 14
   - 9.5 Economic Cost of Disturbances 14

10. Case Study: Turin's Road Network 15
10.1 Study Area 15
10.2 Methodology for assessing the efficiency of the road network to EQIL and earthquake-induced road and building damage. 19
10.2.1 Methodology Overview: 20
10.2.2 Overview of Newmark's method 21
10.2.3 PGA integration and saturation scenarios 23
10.2.4 Calculating PGA Capacity with Fragility Curves: 23
10.2.5 Factor of Safety: 23
10.2.6 Critical Acceleration 24
10.2.7 Newmark's Displacement: 24
10.2.8 Calculating the Efficiency Index: 25
10.3 Methodology for Estimating the cost of disturbances: 26
10.3.1 Risk of Person 26
10.3.2 Risk of Asset 28
10.3.3 Risk due to non-operational availability 28
10.4 DATA SAMPLING: 29
10.4.1 Slope Angle: 31
10.4.2 Soil Parameters: 32
10.4.3 Building and Bridges data: 33
10.4.4 Seismic Intensity: 33
10.4.5 Rainfall intensity: 36
10.5 Assumptions: 37
10.5.1 Infinite slope – Block failure: 37
10.5.2 Allocation of ground parameters: 40
10.5.3 Constants 42
10.5.4 Soil thickness perpendicular to failure surface (t) 42
10.5.5 Saturated thickness compared to the total layer thickness (m) 44
10.5.6 Travel Time and Traffic Demand: 44
10.6 Calculations 44
10.6.1 DS Values: 45
10.6.2 Calculation of the slope angle 45
10.6.3 Calculation of the factor of safety 46

10.6.4 Critical acceleration 47
10.6.5 Newmark's displacement 48
10.6.6 Peak Ground Acceleration: 49
11. Discussion of results: 50
12. Conclusion 51
13. Bibliography 52
14. APPENDICES 56
14.1 Appendix A 56
14.2 Appendix B 57
14.3 Appendix C 58
14.4 Appendix D 63

4. List of Acronyms

ARPA	Agenzia Regionale per la Protezione Ambientale
DEM	Digital Elevation Mode
DS	Damage state
EQIL	Earthquake-Induced Landslides
FS	Factor of Safety
GIS	Geographic Information System
GMPE	Ground Motion Prediction Equation
IM	Intensity Measure
INGV	Istituto Nazionale di Geofisica e Vulcanologia
IRPI	Istituto di Ricerca per la Protezione Idrogeologica
ISPRA	Istituto Superiore per la protezione e la Ricerca Ambientale
LEM	Limit Equilibrium Method
MPS04	Modello di Pericolosità Sismica di riferimento del 2004
OSM	Online Street Map
PGA	Peak Ground Acceleration
PN	Pino Nuovo road
PSHA	Probabilistic Seismic Hazard Analysis
PV	Pino Vecchio road
RIL	Rain-Induced landslides
RN	Road Network

5. List of Tables:

Table 1 Detailed description of the typology for the bridges pertaining to the RN depicted in Figure 5 18
Table 2 Risk variables and their derivation for the calculation of RP: direct impact – standard situation [15] . 27

Table 3 Risk variables and their description for the calculation of RA: direct impact. The calculation of the residual variables is according to Table 2 ..... *28*
Table 4 . Risk variables and their description for the calculation of RD. The calculation of the residual variables is according to Table 2 [15] *29*
Table 5 Calculation of default values of the soil parameters. *39*
Table 6 Different layers of the ground in sample S15 [45] *43*
Table 7 Different layers of the ground in sample S8 [45] *44*
Table 8 PGA value for annual frequency of exceedance [46] *48*
Table 9 First 10 PGA values for each DS level for Path 2 ..... *49*
Table 10 FS and ac of Pino Nuovo road (SS10) *56*
Table 11 FS and ac of Pino Vecchio road. *57*
Table 12 Newmark's displacement of Pino Nuovo road (SS10) *57*
Table 13 Newmark's displacement of Pino Vecchio road. *58*
Table 14 DS values for all the bridges included in our RN [11] *58*

6. List of Figures:

Figure 1 Flowchart depicting the novel framework for the application of the proposed methodology *9*
Figure 2Probability distribution curve of the factor of safety in a specified environment [15] *12*
Figure 3 Visualization of landslides, marked by red dots [38] *16*
Figure 4 a) is the Chieri Hospital, which is the endpoint for our path, and b) is the Gradenigo Hospital which is the start point for our path *17*
Figure 5 Satellite image of a part of the area of interest between the cities of Turin, Pino Torinese, and Chieri, all located in Piedmont, Italy. Sourced from google earth (May 2025) *18*
Figure 6 Flow-chart of the methodology used to compute EQIL and RIL induced landslides *21*
Figure 7 Illustration of the Newmark analysis method. (A) Shows an earthquake acceleration-time history with a critical acceleration of 0.20g, indicated by a horizontal dashed line. (B) Depicts the velocity of the landslide block over time. (C) Charts the displacement of the landslide block over time [42] *22*
Figure 8 Application(Turin): Road network efficiency under a seismic scenario with return period T475 for DS3 ..... *26*
Figure 9 ISPRA-IdroGEO database visualising landslides LPN3, LPN4, LPN5, LPN6 and LPN7 [38] *30*
Figure 10 Numbering of the landslides following the SS10 ..... *30*
Figure 11 Representation of the heights and horizontal distance Lpn4 ..... *32*
Figure 12 ARPA Piemonte database with red dots as survey points, green points as wells [45] *32*
Figure 13 An area of potential road blockage due to landslide or building debris on the road, source Google Earth accessed 24th May 2025 ..... *33*
Figure 14 The grid-based approach to assigning PGA values in Turin [46] *34*
Figure 15 PGA hazard map of Italy using MPS04 [46] *36*
Figure 16 Geometry of the infinite slope surface [52] *38*
Figure 17 Representation of the effective slope length and the deposition area. *39*
Figure 18 Project GIS with buffered samples (radius 500m). *42*
Figure 19 Rainfall in Pino Torinese [50] *44*
Figure 20 Localization of landslide LPN4. ..... *44*
Figure 21 Fragility curves of the Siatista bridge. [11] *45*

7. Introduction

We are living in a period where natural hazards are increasingly becoming unpredictable and deadly. Since the turn of the century, 2.3 billion people have been affected by natural disasters. [1] The occurrence of natural hazards causes damage to our transportation network. The failure of the transportation network can lead to people being cut off from essential services, such as hospitals and supermarkets [2]. Natural hazards are becoming increasingly powerful, and it is becoming more difficult to predict them. These unpredictable natural hazards are placing a significant strain on our existing infrastructure. This decreases the overall efficiency of the road network.

Different natural hazards can lead to the failure of a road network. Still, for our thesis, we will mainly focus on earthquake-induced structural damage (bridges & buildings) [3] that can block roadways and earthquake-induced landslides. Both these hazards are difficult to predict and can lead to road closures for months in severe cases. Between 2021 and 2025, frequent landslides blocked the A83 road for at least one day per week for four consecutive years. In four years, the road was closed 270 full days. The A83 road is the main road from the Scottish Central Belt through local settlements until its termination in the town of Campbeltown in the south-western highlands of Scotland. Located to the west of Ardgartan, situated within Glen Croe, the section of the A83. Communities that rely on this road connection were severely impacted, with the Scottish Tourism industry also taking a hit. [4]

Major disruption is caused by the debris, rock, or earth falling under the influence of gravity. This can happen when buildings suffer damage during an earthquake and the debris fallout blocks the road. Secondly, this can occur when the slope of hills becomes unstable, and the subsequent rockfall blocks the road. [5]This can cause damage ranging from minor issues that take a few hours to clear to complete road blockage and significant damage. That may take months to repair. This causes severe economic loss and even the loss of life. To safeguard our road network against these hazards and risks, we must first understand how they work [6]

This thesis takes forward the work of Maxim's thesis titled "A framework for assessing the earthquake-induced landslide resilience of a road network in Turin, Italy".

This research aims to study and map the behavior of the road network under the combined influence of earthquake-induced landslides, debris fallouts, and bridge damage. Furthermore, we propose a framework to calculate the annual loss resulting from road closures due to natural hazards. This will give us a better understanding of how these hazards not only affect the physical infrastructure but also the communities that rely on it for their everyday travel. This will help city planners to plan and ensure that preventive measures are taken, such as strengthening the structures along the road, whether it be buildings or slopes. This thesis used the data provided by the istituto superiore per la protezione e la ricerca ambientale ISPRA and and agenzia regionale per la protezione ambientale (ARPA) Piemonte. These databases contain information on previous landslides, including detailed data on their locations and causes. By thoroughly analysing these data, a deeper understanding of the patterns and frequency of landslides in the region can be gained. This helps to understand the risks better and develop accurate prediction models. The methodology combines peak ground acceleration (PGA) data with saturation scenarios to assess slope stability. The PGA is a measure of

the intensity of ground shaking during an earthquake and plays a crucial role in determining the probability of landslides. Saturation scenarios help understand how slope stability changes under different levels of soil saturation due to rainfall. By combining these two methods, potential landslide risks can be estimated under various conditions. The data for the buildings along the selected routes was provided by the Divisione Infrastructure e Mobilità–Servizio Ponti, Vie d'Acqua e Infrastrutture of Comune di Torino. For this study, the road network chosen includes two primary routes. These routes run along the south of Turi, where most landslides have occurred in the past. Pino Nuova (SS10). This route is one of the most important roads in the region as it is the fastest connection between the towns of Sassi and Pino Torinese. Pino Vecchio Road, the second-fastest connection.

8. Multi-Hazard Risk Assessment on Road Infrastructure.

Natural hazards are becoming increasingly intense and unpredictable; combining this with an ever-growing urban population is a recipe for disaster. Our modern economies are built around the fast transportation of goods and services, and road infrastructure is a vital component of this [7]. However, our road infrastructure is vulnerable to the impacts of climate change and natural hazards. Events such as earthquakes, prolonged heavy rainfall, floods, and landslides can cause significant damage to the road network, leading to long-term disruptions in mobility and access, complicating emergency responses, and increasing recovery costs. [8]. The resilience of road infrastructures, defined as the capacity to anticipate, absorb, adapt to, and rapidly recover from such events, is therefore a critical focus in transportation engineering and planning. To understand all this, it is first essential to familiarize oneself with and review the existing literature on this topic.

9.1 Impact of natural hazards on the Road Network

Natural Hazards, such as seismic activity, intense rainfall, and debris flow, pose a serious threat to our road network. This becomes particularly important during emergency events, when the road network serves as a crucial pathway for Emergency service providers. If the road network itself becomes incapacitated during a natural hazard event, the entire response to any emergency will become significantly more difficult. For this reason, it is crucial to calculate and understand the resilience of a Road network during a hazard event [2] [9]. For example, seismic activity can disturb the surrounding soil, causing soil erosion and landslides, with debris falling onto the road. At the same time, it can cause structural damage to roads and bridges. That can sometimes take months to repair, and often, the cost of these repairs is in millions of euros. The physical damage to infrastructure is one thing. Still, the socio-economic loss to communities and businesses that rely on the road network for their daily lives is often overlooked when calculating the cost. [10]

9.2 Literature Review:

In this thesis, the analysis relies on two things: researching earthquake-induced landslides and making a framework for modeling them, and secondly, understanding how buildings and bridges in our RN (road network), and what impact it has on the efficiency index of our road network. For the

earthquake-induced landslides, help was drawn from a thesis titled “A framework for assessing the earthquake-induced landslide resilience of a road network in Turin, Italy.” This thesis provided us with the framework to model EQIL (Earthquake-induced Landslides). To assess buildings and bridges during a seismic event using the framework, we first needed to understand the fragility curves. With these curves, we can calculate the Peak Ground Acceleration Capacity of a structure (PGAcap) for each bridge [11] and building [12]. For bridges, the curves developed by Moschonas [11] were used, while for the building’s fragility curves provided by Rosti et al. [12] were used. The Moschonas paper used the pushover analysis technique to make the pushover curve. The damage state is assessed primarily in terms of parameters from the pushover curves of the generic bridges, along with some local quantities, such as bearing deformation. Finally, Peak ground acceleration demand (PGAdem) for the under-study area can be calculated from INGV (Istituto Nazionale di Geofisica e Vulcanologia). The Monte Carlo simulation is used to create an efficiency index. We use the Monte Carlo simulation because it provides not just one solution, but multiple solutions, and it is also useful because the Monte Carlo simulation models uncertainty in the input parameters.

9.3 Efficiency Index of Road Network:

An efficiency index calculates the engineering efficiency of a road network (RN). The Efficiency Index (Ei) is a dimensionless value, ranging from 1 to 0, where 1 indicates 100% functionality and 0 indicates complete failure. Erm tells us how a road network responds to a hazardous event. For example, if the ERM is 0.79 after a dangerous event, it means that the efficiency of the road network in transporting traffic at the pre-hazard speed has decreased by 21%. The reason I mention speed is that the average transportation time between two nodes is also considered, as the efficiency of a transport system is not just about connecting point A to B, but also about connecting them promptly [3] [13]. By using an efficiency index, we can identify the critical nodes in our road network (RN). By utilizing this approach, we can minimize the system’s vulnerability by strengthening the weak nodes in our RN. [14]. The primary objective of this thesis is to develop an efficiency index that can simultaneously account for multiple hazards. In our case, we will consider EQIL (earthquake-induced landslides), debris falling from buildings along the RN (road network), and bridges along the RN that become structurally damaged.

9.4 Methodology:

This thesis proposes a methodology for the multi-hazard risk assessment of road networks (RN) and calculates the economic cost of such disturbances. Our approach considers the built environment and the impact of the terrain on the capacity of a road network (RN) after a seismic event. Simple mathematical relationships are created to calculate road network (RN) efficiency after a seismic event. [3]. To make this efficiency index, the damage to overall buildings, bridges, and terrain along the RN is studied. The terrain was extensively studied in the thesis “A framework for assessing the earthquake-induced landslide resilience of a road network in Turin, Italy “to get information about past landslides and potential landslide-prone sections in our road network (RN). The uniqueness of this framework lies in its ability to assess the various factors that influence overall RN efficiency. The identification of urban critical node pairs, all potential road connections, and their pertinent characteristics, such as travel time, are all included in RN modelling. At the same time, hazard-based seismic scenarios consider site-specific seismic intensities and model events with varying

return periods. Bridge typologies are categorized, and the most significant factors affecting building vulnerability are identified during the seismic vulnerability modeling phase. By combining these components, the suggested framework connects the transportation and structural engineering aspects and offers a methodical way to assess how effective urban RNs are during seismic activity. Additionally, a new framework was developed to calculate the cost of these disturbances. The framework considers the total traffic in the road network, including the probability of fatality and other factors. [15] . It works on Probabilistic seismic hazard while reducing computational cost. A flow chart is presented in Figure 1, depicting the proposed methodology.

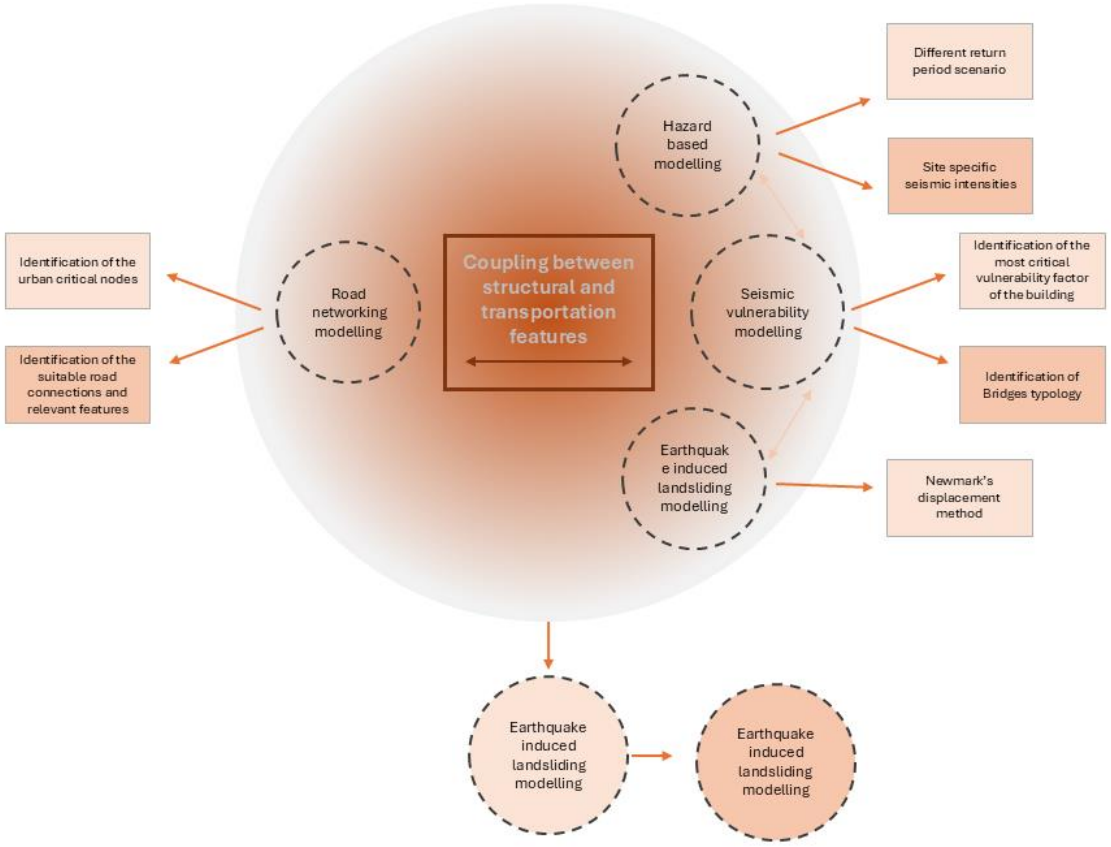

Figure 1 Flowchart depicting the novel framework for the application of the proposed methodology

9. Hazard Modeling and Risk Assessment

We must first model our road network (RN) to simulate risks and identify hazards. QGIS v3.38 is used to accomplish this. QGIS is a geographic information system (GIS) software program. This integrates a variety of data sources, making it easier to obtain and georeference specific data. The RN is represented by a graph consisting of a unique set of nodes and arches, the latter of which resemble roads and connections. QGIS enables the precise identification of the location and typology of every

building and bridge along the road network. The characteristics that are most impacted by an earthquake are used to categorize bridges. For example, the kind of deck, pier, and connection between the pier and the deck. Similarly, buildings are classified based on their height and number of floors. For simplifications, it is assumed that all buildings are made up of reinforced concrete (RC)

9.1 Built-Up Environment Risk and Hazard Assessment

For the calculation of the Risk posed by buildings and bridges to the road network, an alternative strategy was used. In this approach, earthquake scenarios are simulated by integrating hazard analyses with fragility models of buildings and bridges. This approach is adopted from a research paper, "Efficiency Assessment of Urban Road Networks Connecting Critical Node Pairs under Seismic Hazard. " [3]. For this, we made a seismic scenario labelled Sc475. This corresponded to a return period of T475=475y. This is done to assess the seismic demand in terms of peak ground acceleration. This PGAdem is the seismic action that will be imposed on the structures within the RN. So, in each simulation, we will subject the buildings and bridges in the road network to the corresponding PGADem. Each bridge and building is assigned a logic value of 1 if it meets the following condition.

$$PGAdem > PGAcap,$$

Equation 1

This would mean that the corresponding bridge or building would be damaged after a seismic event, as the demand exceeds its capacity. And if they don't meet the criteria mentioned above, they will assign a value of 0.

In Equation (1), the seismic demand and capacity are modelled as follows:

$$PGAdem = \mu 50 \exp(\beta A),$$

Equation 2

$$PGAcap = M50 \exp(BA),$$

Equation 3

Where A is a uniformly distributed pseudorandom scalar, β and B represent their standard deviations, and μ50 and M50 represent the 50th percentile of the lognormal distribution of capacity and demand, respectively. The suitability of the assets in question serves as a guide for the distribution decisions. The distributions created by Moschonas et al. [10] for bridges are used in Section 3, while Rosti et al. [11] are taken into consideration for buildings. Following each simulation, roads with at least one structure designated with a value of 1 will be considered disrupted, which will lower the operational efficiency of the RN, as explained in the subsequent paragraph. Previously,

this analysis was conducted only for DS3, but now we have extended it to DS1-DS5 and compared the results.

In the context of urbanization, an RN's effectiveness is crucial to reaching the targeted resilience [16] and, in a sense, sustainability, for a city. The speed at which roads in a particular urban setting connect vital nodes, like hospitals, is known as efficiency. To determine an RN's efficiency, the demand for traffic flow was taken to be constant [17] regardless of any alterations brought about by the seismic event. Therefore, the following formula is used to evaluate the efficiency of the ith road, represented by Ep, i, for an RN with n roads:

$$Ep, i = 1 - tp, i/tref$$

Equation 4

Where i ranges from 1 to n, tp represents the mean travel time of the ith road, and tref denotes the maximum time required to connect the two critical nodes of interest. In the application reported in Section Application and Results of this paper, tref is selected as the time threshold, commonly referred to as out-of-hospital time. [18], Specifically referring to the patient transport phase. The mean travel time of the ith path within the road network is calculated as follows:

$$Tp, i =- Lp, i/vm, i,$$

Equation 5

where Lp represents the path length and vm is the mean velocity. Information on LP and VM in Equation (5) is sourced from QGIS. When selecting between ground emergency medical services (EMS) (EMS) and helicopter EMS for transportation between two hospitals or from a hospital to any other critical node, hospital managers must decide which route offers optimal intervention for ground EMS. [19] [20]. To facilitate this decision-making process, the time of travel (Toh) is defined as the maximum travel time, tp, max, among n suitable routes, with an additional 50% accounting for uncertainties related to fluctuating traffic conditions and road availability. [18]. This is expressed as follows:

$$tooh = 1.5\ tp, max.$$

Equation 6

The goal is to determine how the RN's efficiency changes in a post-event scenario because a post-disaster assessment is conducted. The efficiency Ep of a road will be zero whenever it is indexed with a single digit during a simulation, signifying disruption. Consequently, the efficiency associated with the RN, represented by the symbol ERN, for a generic jth simulation is the maximum efficiency Ep,j within the RN among the available roads that are marked with only 0 digits. This enables the assessment of how RN efficiency varies in response to seismic activity.

9.2 Landslide Risk and Hazard Assessment

Numerous variables can cause landslides, which are complicated geological phenomena that all combine to destabilize the slope. Three conditions of slopes are thus considered, shown in Figure 2: stable, marginally stable, and actively unstable. Each type defines a distinct probability of landslides occurring, depending on different controlling variables. It is deemed unlikely that the initial class, stable slopes, will produce a trigger big enough to cause the slope to fail or move. As the forces resisting slope movement are greater than the forces favoring failure, such areas have high safety factors. Stable slopes are usually not prone to landslides except when their conditions become drastically altered [21].

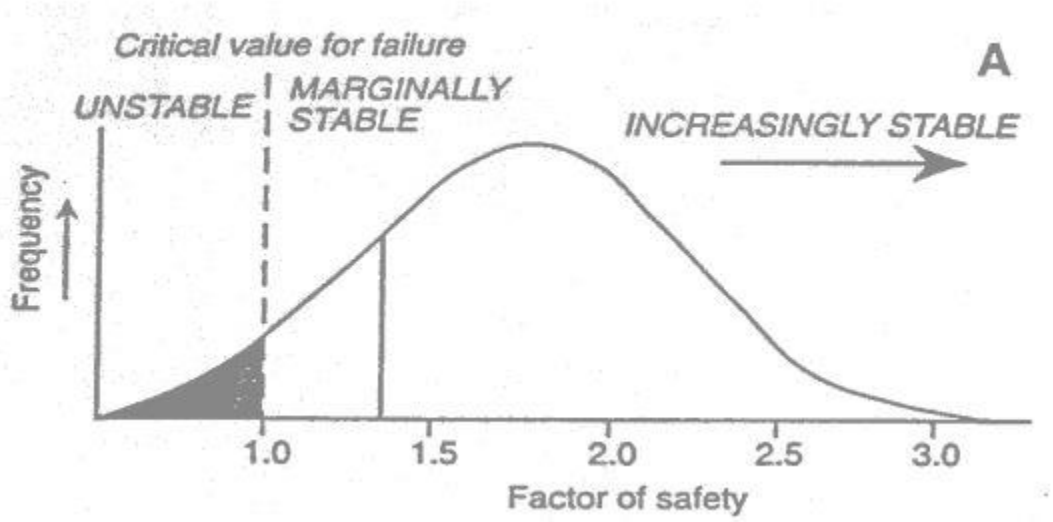

Figure 2 Probability distribution curve of the factor of safety in a specified environment [15]

Marginally stable slopes are those where the current environmental conditions are likely to produce a trigger that could lead to failure. There is more than one factor that can turn a stable slope into an actively unstable one. When a slope fails, it leads to a landslide that occurs when several unfavorable circumstances, both man-made and natural, come together. In regions of actively unstable or marginally stable slopes, where the delicate balance is easily upset and may cause sudden and sometimes catastrophic slope failure, such seismic activity is especially pertinent [22]. Rainfall influences slope stability, primarily due to hydrological changes in the soil. Prolonged or heavy rainfall episodes compromise the stability of the slope, as they can raise pore water pressure and reduce the frictional resistance of the soil particles. Furthermore, saturation caused by heavy rainfall intensifies the loading on the slope material by raising hydrostatic stress and allowing movement [22]. This process is essential for converting marginally stable slopes into actively unstable ones, particularly when the soil's capacity to absorb water is exceeded. [23]. The goal of landslide hazard assessment is to identify and characterize geographical areas susceptible to landslides, with an emphasis on the likelihood and spatial distribution of such events. This involves a systematic evaluation of the potential for landslides to occur in a particular area. It considers several geological, topographic, and environmental conditions that contribute to the initiation of

landslides. We receive hazard maps, which graphically depict the area vulnerable to landslides due to this. Susceptibility Mapping produces maps that show the probability of landslide occurrence in different regions, based on terrain characteristics such as slope angle, soil type, and vegetation cover. This can be done with the help of GIS. We can use GIS to create models that can handle all the information regarding slope angles, soil types, and other relevant factors, and then represent the data in a clear and easily understandable form. [24] Hazard Zonation: Classifying the landscape into zones of varying landslide hazard levels, helping planners and engineers prioritize areas for mitigation efforts.

9.2.1 Landslide Risk Assessment

Evaluation of landslide risk considers the possible effects of landslides on infrastructure, economic activities, and human life. Coupled with the vulnerability of the elements at risk, we multiply the probability of landslide occurrence to determine the risk. Facilities such as Viaducts and bridges are particularly vulnerable to deteriorative structural decay since they tend to be built in problematic terrain where seismic hazards, along with landslides and other hydrological risks, prevail. In the past, it has emerged that landslides are one of the major causes of bridge failure. Both because of the unpredictability of landslides and the complex conditions that trigger them. [25] Landslides can act in a completely hidden manner without any warning signs. Bridges and viaducts are not designed to withstand huge lateral loads, especially at the piers. They are load-bearing structures. In some situations, depending on the landslide displacement rate, the piers are affected by the movement of debris or mud and show signs of damage. This can lead to the collapse of the structure, and it has indeed happened in the past [26]. Estimating the possible outcomes and creating plans to mitigate the negative effects are the objectives. Important elements of landslide risk assessment include: Analysis of Risk, which involves assessing the potential negative impact of landslides, such as fatalities, infrastructure damage, and financial losses. [27] [28] This entails assessing how vulnerable and exposed people and assets are in locations that are prone to hazards. Calculating Quantitative Risk: estimating the probability and impact of landslides using statistical and probabilistic techniques. To more precisely forecast future events, this often involves combining historical data with real-time monitoring. Danger management is the process of creating and putting into practice strategies to lower the danger of landslides, such as early warning systems, land-use planning, and engineering solutions (such as drainage systems and retaining walls). Nowadays, early warning systems for landslides (LEWS) are gaining traction worldwide. [29]. From now on, the data from this thesis can be used to create LEWS.

9.3 Earthquake-Induced Landslides:

Seismic activity causes these landslides, and several variables, including ground shaking, geological conditions, and slope characteristics, influence the frequency of their occurrence. Because of the severe shaking of the ground caused by earthquakes, which accelerates the soil horizontally, landslides can destabilize slopes and lead to their failure. The magnitude and duration of the earthquake, the distance from the epicenter, and local geological and topographical conditions are the primary factors influencing earthquake-induced landslides, also known as EQILs. The cohesiveness of rock and soil on slopes can be weakened by seismic waves, resulting in abrupt and frequently disastrous landslide events.

Peak Ground Acceleration (PGA), which measures the magnitude of ground shaking at a particular location, specifically the moment of the strongest shaking during an earthquake, is a crucial parameter in this context. Stronger shaking is associated with higher PGA values, which increases the risk of landslides [27]. Areas with high seismic activity, such as the Pacific Ring of Fire, the Himalayas, the Andes, and other tectonically active mountainous regions, are particularly important for assessing the risk of earthquake-induced landslides [28].In these areas, the combination of frequent seismic events and steep, unstable slopes creates a high risk for landslides. In these places, therefore, there will be higher PGA values and a decrease in the factor of safety. Accurate assessments in these regions can help mitigate the impacts of such events through better planning and early warning systems [30]. Numerous attempts have been made to estimate seismic-induced landslides at the regional level. The Newmark displacement approach is a widely used method for evaluating landslides triggered by earthquakes (Newmark 1965) [31]. This method provides a measurement, DN, of the permanent displacement that a seismic event along a contact creates on a rigid block surface; it is a helpful tool for defining the slope's behavior due to seismic action, but it does not always predict the slope's displacement. Some other methods define, in terms of susceptibility factors, the occurrence of a sliding slope, such as the Mora–Vahrson method (Mora and Vahrson 1993, 1994). However, for this thesis, we will consider Newmark's displacement method. [32]

Wilson and Keefer [33] propose critical values for DN corresponding to some displacement thresholds; they suggest a value of 10 cm to define coherent landslides and 2 cm for disrupted landslides. Therefore, for our thesis, we will set the DN equal to 10 cm.

9.4 Risk Assessment

The fragility curves reported in Moschonas et al. [11] for bridges and Rosti et al. [12] for buildings are used to assess the structures' PGA capacity, or PGAcap. This procedure enables the determination of the damage state (DS) that each structure has sustained. Because going over a certain DS threshold could cause the road to be blocked, it is crucial in this situation to carefully define the practical implications of each DS. Moschonas et al. [11] discuss bridges. They employed four DSs in addition to the no-damage state (DS0): failure/collapse (DS4), major/extensive (DS3), moderate (DS2), and minor/slight (DS1). Moschonas et al. utilized a variety of research, including that by Choi et al. [34], Erduran and Yakut [35], and Basöz et al. [36], to thoroughly interpret these DSs. Rosti et al. [12] established five DSs for RC buildings based on the EMS-98 macroseismic scale [37]. No damage (DS0), insignificant to negligible damage (DS1), considerable to serious damage (DS2), very serious damage (DS3), partial collapse (DS4), and collapse (DS5) are the DSs that correlate to the various levels of damage to vertical structures. After a meticulous evaluation, the authors have determined that reaching a PGA capacity corresponding to an intermediate DS, between DS1 and DS2, is adequate to trigger road interruption in the case of Scenario Sc50 with a return period of Tr = 50 years. Conversely, reaching DS3 would lead to road interruption in the case of Scenario Sc475 with a return period Tr = 475

9.5 Economic Cost of Disturbances

Assigning a monetary value to the drop in road network (RN) efficiency is important for a couple of reasons for one it tells us how each hazard events impact the economy of an area and how

communities that rely on the road network (RN) for their daily travel are affected when hazard event take place. And secondly, it enables us to prepare more effectively and direct funds and resources for the better rehabilitation of the affected areas. For this thesis, we adopted a deterministic approach to calculate the economic cost of a seismic event.

We calculate the risk of landslides, debris fallout, and bridge collapse due to a 475-year earthquake event and then use that risk to estimate the associated costs. This is done by calculating the risk of person (risks posed to human life due to seismic events), Risk of asset (risk posed to public, private buildings and the infrastructure) and the risk of non-availability (the risk of road being blocked and the economic cost associated with the road being blocked). A specific cost is assigned to each risk, and then the total cost is estimated based on these risks. [15]

10. Case Study: Turin's Road Network

This chapter presents the methodology and results of the landslide modelling done for the chosen road network (RN) in the Torino area. The study's primary objective is to assess the stability of the slope, evaluate the damage to bridges and buildings along the road, and determine how this damage affects the efficiency index of the road network. And finally, to calculate the cost of such disturbances. Along two important roads, Pino Vecchio Road and Pino Nuovo (Main Road). The analysis attempts to assess the risk of landslides under various circumstances by combining geological, hydrological, and seismic data, combiningthereby combining the landslide risk with the the risk of the bridge being damaged and debris falling out due to a seismic event. It also provides an opportunity to suggest mitigation techniques to improve the road infrastructure's resilience. The study area, data sampling procedure, and techniques used to model and evaluate landslide susceptibility are all detailed in the following sections.

10.1 Study Area

This study, shown in Figure 3, is in the northwestern Italian region of Piemonte. This centers around the Strada Statale (SS) 10, a significant suburban thoroughfare. This road segment of interest extends from the Sassi and Reaglie neighbourhoods on Turin's outskirts to the municipality boundary between Pino Torinese and Chieri. A section of the Collina Torinese (Turin Hills) is included in this area. The SS10 serves as the primary route connecting Turin and the other municipalities on its southeast side from the standpoint of the road network. This study focuses on a specific region around Turin, Piemonte, Italy, to analyze the road network connecting two critical points: Gradiengo Hospital in Turin and. Both points are located outside the center of Turin, specifically in the South of the city. The area was selected due to its strategic importance for transport between Chieri and Torino, serving both medical and general transportation needs. The region under study is situated within the metropolitan area of Turin, located in the Piedmont region of northwestern Italy. Turin, the capital city of Piemonte, is a major cultural and economic hub, surrounded by a network of towns and municipalities. The specific focus is on the road network connecting Sassi, a suburb of Turin, to Pino Torinese, a nearby town situated on the hills overlooking the city. Not only because of its strategic location in Piemonte itself, but also the density of landslides makes this region interesting for research. One of the key points in determining the region was its susceptibility to landslides.

Regions prone to these phenomena need more attention. Therefore, databases were used to identify the locations of these more sensitive regions. The database used in this research is Istituto Superiore per la Protezione e la Ricerca Ambientale (ISPRA). They provide a database of registered landslides for the entire country. Figure 3 illustrates this, where each red dot represents a landslide that occurred in the past and was subsequently recorded by ISPRA. As is visible, no registered points are visible in the city centre. However, in the south below the city, this is the case; the density and thus the number of already occurred landslides in this region is the highest, and thus also interesting for this study to focus on.

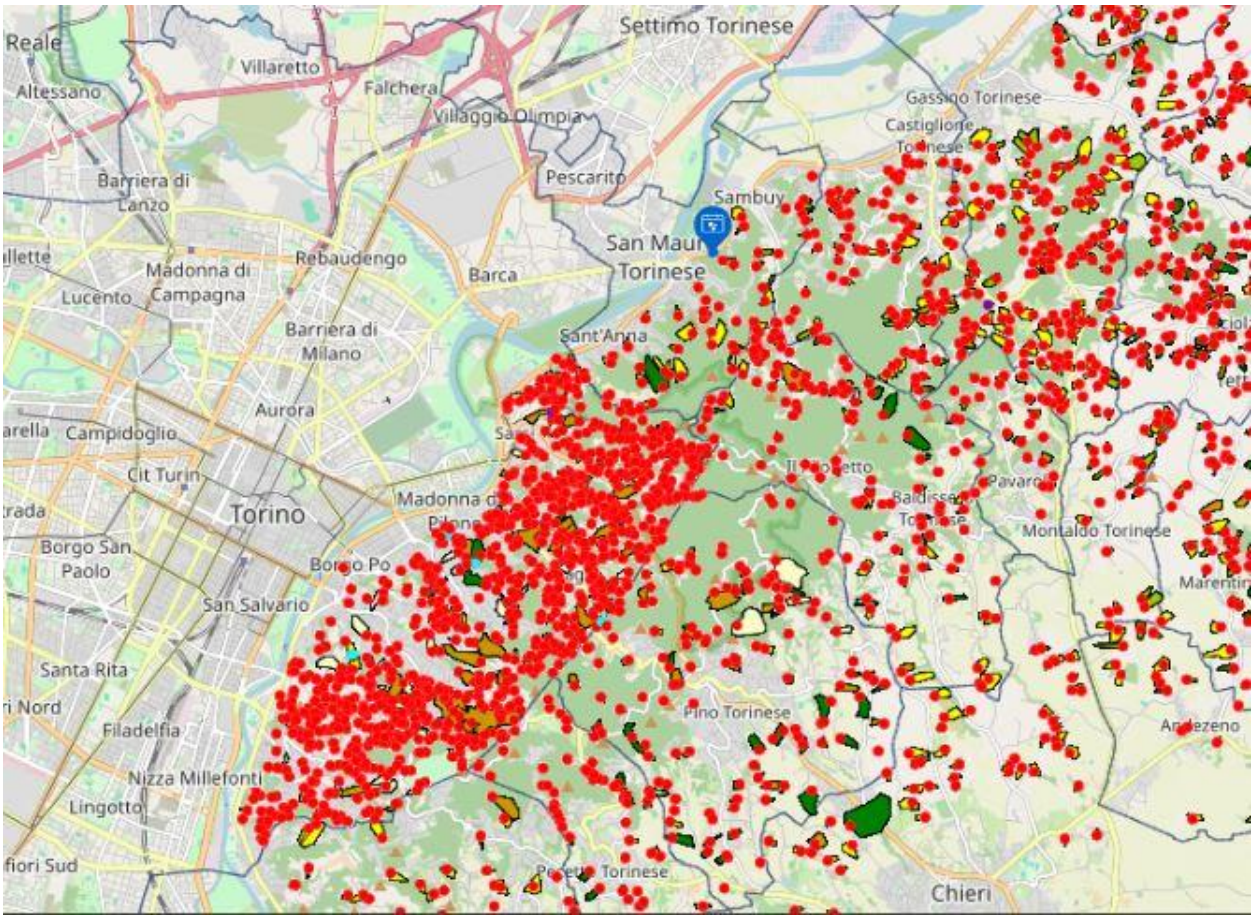

Figure 3 Visualization of landslides, marked by red dots [38]

There are 14 facilities in total, including 13 viaducts (one of which is a flyover) and one tunnel, on the chosen SS10 segment. The latter is the primary tunnel in the region surrounding Turin. That tunnel, which was constructed between 1949 and 1956 to facilitate the transfer of people and products from Turin to Asti, is a prime example of post-war infrastructure. Except for one short-span monolithic RC block, all viaducts, aside from the overpass, were constructed simultaneously and share the same structural design: a simply supported girder deck with four longitudinal prestressed RC girders. Due to interference with "Strada Tetti Bertoglio," a subsidiary road, the flyover on the SS10 road is an RC bridge. It has two significantly shorter lateral spans and a longer central span. There are fewer ways to get from one place to another in such a road network than in an urban setting. The road known as Corso Torino on the Pino Torinese side and Corso Chieri on the Turin side are by far the most

important alternative among the secondary routes that might be utilized. Locals also refer to this as the Strada del Pino Vecchio, or the old road through Pino Torinese, as opposed to the SS10, which is locally referred to as the Strada del Pino Nuovo. Crucially, this ancient route crosses the hills above the tunnel, following the natural curves of the hill slopes without encountering any bridges along its entire length, and passes through the historic town of Pino Torinese, a small but comparatively populous village.

Figure 4 a) is the Chieri Hospital, which is the endpoint for our path, and b) is the Gradenigo Hospital which is the start point for our path

The two paths considered here encompass the main option for a driver to move from the starting point (Pino Torinese-Chieri boundary) to the endpoint (Gradenigo Hospital). Importantly, the critical connection representing the southern point can be seen as indicative of a hospital-to-hospital route, as in the case of Application #1, minus a time constant. All traffic moving from Chieri Hospital (Figure 4To reach Gradenigo Hospital in Turin would need to follow the same road, regardless of the two optional paths, up to this point. The two paths begin to diverge only after the critical node. For this reason, this shared road segment (indicated by the blue line in Figure 5) did not affect the comparison between the two options; therefore, it was not considered in the calculations.

Figure 5 Satellite image of a part of the area of interest between the cities of Turin, Pino Torinese, and Chieri, all located in Piedmont, Italy. Sourced from google earth (May 2025)

The first option available to the driver is to follow SS10, passing through the road tunnel and the series of viaducts described above. The second option is to bypass them along an older route. Then, coming from SS10 or Corso Chieri into the Sassi neighborhoods, the driver must cross the Po River. Again, the two chokepoints limit the possible routes. One can cross the Po River into Corso Belgio (using the so-called Ponte Sassi Bridge, a historical multi-span RC arch bridge) and then pass through the Vanchiglia and Vanchiglietta neighborhoods. Alternatively, one can use the Corso Regina Margherita Bridge, which is directly in Vanchiglia. The latter bridge, shown in Figure 8, represents the most important infrastructure along the way. This infrastructure is an RC arch bridge built between 1970 and 1972, designed with the extensive use of post-tensioned DYWIDAG cables. It is also subjected to high daily traffic loads, with an average daily traffic of 2715 vehicles. Therefore, Path 1, colored orange in Figure 5, has only one bridge, i.e., Corso Regina Margherita Bridge (hereinafter, V1-T), and 384 adjacent buildings, the collapse of which may produce road disruption. Paths 2, in yellow, in Figure 5, add to these 13 viaducts located on SS10 (V3-T to V15-T). Path 2 (ss10 then Ponte Sassi Bridge) includes 310 buildings in total. The bridges that are part of the paths of interest are briefly described in Table 1. The Municipality of Turin oversees the first nine viaducts of SS 10 (V3-T to V15-T) and the two river crossing bridges. The boundaries of the Pino Torinese municipality area encompass the other four SS 10 viaducts (V12-T to V15-T). Because SS 10 intersects with a subsidiary road, only one viaduct (V8-T) is a flyover rather than part of the real path

infrastructure. Since its possible collapse would still disrupt traffic on the path below, this has been included. The Municipality of Turin performed reinforcement interventions on seven SS 10 viaducts (V3-T to V7-T, V9-T, and V10-T) from 2012 to 2020, with the replacement of longitudinal girders.

Table 1 Detailed description of the typology for the bridges pertaining to the RN depicted in Figure 5

Bridge Name	Bridge Typology	Number of spans
V1-T	River-crossing post-tensioned RC arch bridge	One longer central span and two significantly shorter lateral spans
V2-T	River-crossing RC arch bridge	three spans of equal length
V3-T	Simply supported viaduct with prestressed RC girder deck	nine spans
V4-T	Simply supported viaduct with prestressed RC girder deck	Three spans
V5-T	Simply supported viaduct with prestressed RC girder deck	Single span
V6-T	Simply supported viaduct with prestressed RC girder deck	nine spans
V7-T	Simply supported viaduct with prestressed RC girder deck	two spans
V8-T	Overpass viaduct with RC deck	One longer central span and two significantly shorter lateral spans
V9-T	Simply supported viaduct with prestressed RC girder deck	Five spans
V10-T	Simply supported viaduct with prestressed RC girder deck	three spans
V11-T	RC monolithic deck	Single span
V12-T	Simply supported viaduct with prestressed RC girder deck	Four spans
V-13T	Simply supported viaduct with prestressed RC girder deck	six spans
V14-T	Simply supported viaduct with prestressed RC girder deck	two spans
V15-T	Simply supported, prestressed RC girder deck with seven spans (end-span RC deck replaced by mixed steel girder-RC deck)	

10.2 Methodology for assessing the efficiency of the road network to EQIL and earthquake-induced road and building damage.

The methodology applied for the computation of landslide hazard assessment, including both Earthquake-Induced Landslides (EQL) and Rainfall-Induced Landslides (RIL), integrates direct Peak Ground Acceleration (PGA) values from Probabilistic Seismic Hazard Analysis (PSHA) with a focused analysis on saturation scenarios within the soil. This comprehensive approach is shown in the flowchart in Figure, which sketches the sequential steps and interactions between different parameters and datasets.

10.2.1 Methodology Overview:

To ensure that the seismic data used is the most recent and region-specific seismic hazard data, requiring no additional adjustments, the analysis begins by extracting PGA values directly from PSHA (Probabilistic Seismic Hazard Analysis). The validity and position of the seismic data depend significantly on the direct implementation of PGA. By defining a set of saturation scenarios, the method considers both the hydrological influence on slope stability and the inclusion of seismic data. The most favorable and unfavorable cases, namely. The saturation parameter m, where m = 0 is the ideally dry situation and m = 1 is the fully saturated condition, defines these scenarios. This dual strategy encompasses the ability to assess how the soil will behave at different moisture levels, a factor that significantly influences its shear strength and, in turn, the stability of the slope. Synthesizing these data points involves several important steps: [39].

1. **PGA Integration:** Utilizing PGA values from PSHA (Probabilistic Seismic Hazard Analysis) as a basis for seismic input.

2. **Defining the road network:** The RN is modelled as a QGIS-v3.38 informed graph. The RN is represented by a graph composed of a discrete set of nodes and arches, the latter of which simulates roads. The network is conceptualized as the framework upon which urban services are organized.

3. **Using the DS to calculate the PGA cap**: PGA capacity is the capacity of a building or a bridge to withstand a certain level of PGA (peak ground acceleration). With the help of fragility curves, we know how much damage a structure would incur at a given PGA.

4. **Saturation Scenarios:** Analyzing the impact of different saturation levels on soil stability by manipulating the m value according to predefined best and worst-case conditions.

5. **Factor of safety Calculation:** Determination of the factor of safety of the slope, both in dry and saturated conditions, which is one of the key criteria for landslide susceptibility.

6. **Critical Acceleration:** Computation of the essential acceleration of the slope, which dictates the minimum horizontal acceleration required to initiate slope movement. The parameter is relevant for assessing the seismic resilience or vulnerability of the slope under different **saturation conditions.**

7. **Displacement analysis:** Determining the Newmark's displacement for the slope, the amount of potential movement due to seismic activity. ThisThis process involves applying critical acceleration to see how the slope responds to the seismic forces introduced.

8. **Calculating the Efficiency Index:** After determining the Newmark's displacement for the slope, we calculate the efficiency index of the road network, considering the DS values for bridges and buildings, as well as Newmark's displacement.

9. **Cost of disturbances caused by the seismic event:** After calculating the efficiency index of the road network in an its ideal condition and then after a seismic event, we attempt to assign a monetary value to the efficiency drop.

This methodology not only ensures a detailed assessment of landslide risks under varied environmental conditions but also provides a clear framework for integrating seismic and hydrological data into a cohesive hazard analysis model. The approach aims to effectively identify areas at risk of landslides due to both seismic activity and rainfall, offering a robust tool for disaster risk management and mitigation planning in susceptible regions.

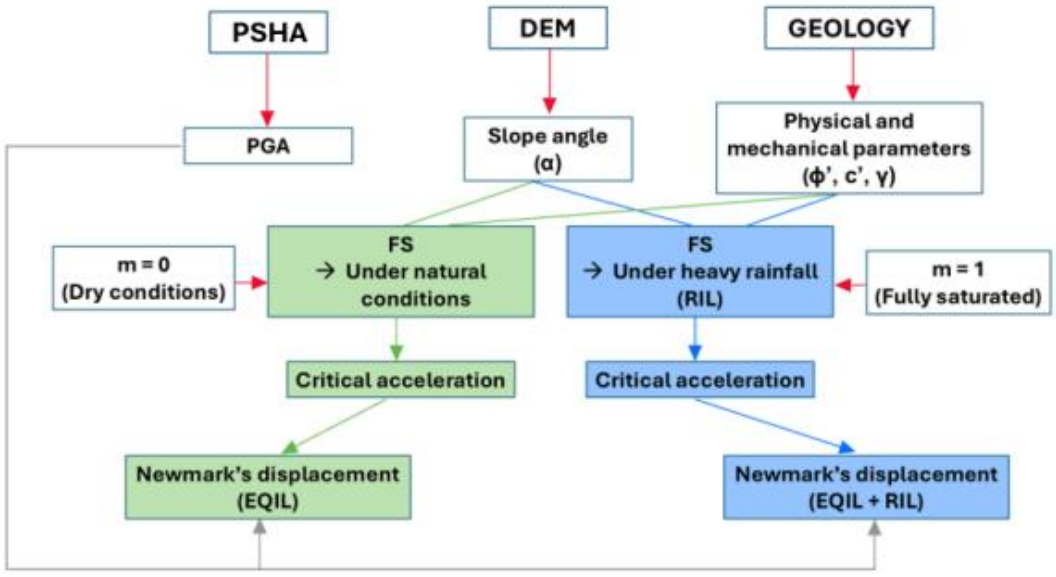

Figure 6 Flow-chart of the methodology used to compute EQIL and RIL induced landslides

10.2.2 Overview of Newmark's method

The efficiency of this road network is determined using Newmark's approach. One popular analytical technique for determining whether slopes are stable under seismic loads is Newmark's displacement method. It simulates a landslide caused by seismic activity as a rigid friction block on an inclined plane that experiences the same accelerations as the slope under the model. The technique is based on the idea that the block moves when the total of the driving forces, both static and dynamic, exceeds the block's shear resistance. [40]

A block will begin to move when the seismic forces act on it above a threshold acceleration, which is a critical level. Several assumptions are made by the methodology used to forecast this

movement. The block is regarded as a hard object that does not bend or change shape, as it first assumes rigid, perfectly plastic behavior. After it begins to move, its internal structure remains unchanged. Second, the block is anticipated to glide along a clearly defined sliding surface. This surface is well-known and transparent. Third, it assumes that there is a small loss in shear resistance during shaking, which means that the block's shear resistance or resistance to movement does not drastically diminish during earthquake-induced shaking. Even as the block begins to move, its resistance to movement essentially stays the same. Lastly, the block will only move permanently if the earthquake forces (dynamic stresses) are larger than the forces holding it in place (shear resistance). This is because permanent displacement occurs only when the dynamic stresses exceed the shear resistance of the material.

In conclusion, the technique assumes that if the earthquake pressures are strong enough, a block of rock or dirt will move. The block is handled as though it were a solid object travelling along a certain surface, and shaking does not significantly reduce its strength. Only when the earthquake forces exceed the resistance forces will the block move. [41]

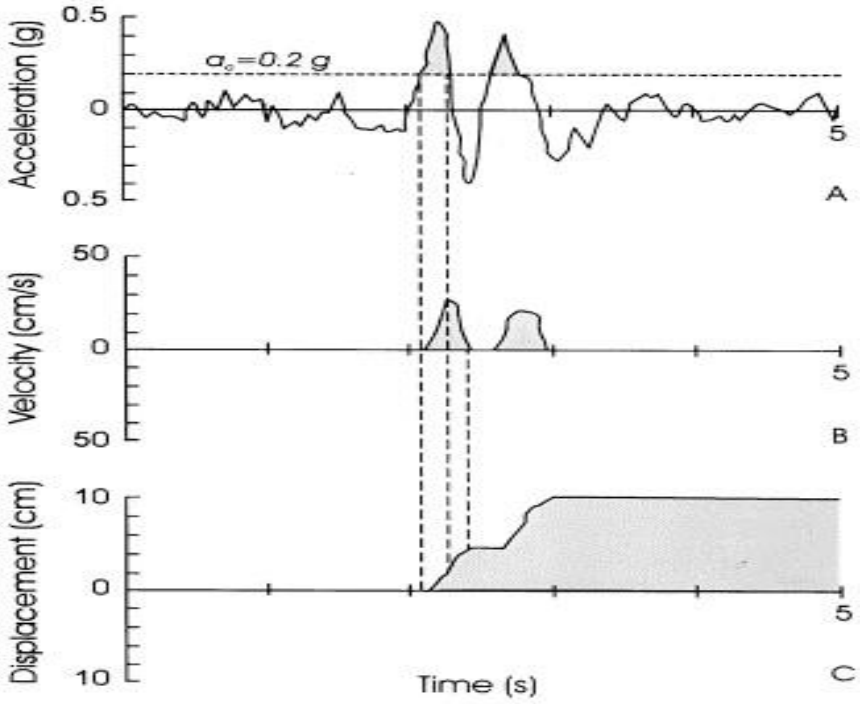

Figure 7 Illustration of the Newmark analysis method. (A) Shows an earthquake acceleration-time history with a critical acceleration of 0.20g, indicated by a horizontal dashed line. (B) Depicts the velocity of the landslide block over time. (C) Charts the displacement of the landslide block over time [42]

It is important to note that Newmark's method, while useful, employs a simplified model of rigid body displacement. As such, it does not aim to predict exact landslide displacements observed in the field but rather serves as a valuable indicator of potential slope performance during seismic events. This method's strength lies in its ability to provide a comparative index of slope stability under various seismic conditions.

10.2.3 PGA integration and saturation scenarios

The initial step, pivotal in methodology, is integrated into the fifth step involving Newmark's displacement, as illustrated in the flow chart depicted in Figure 6. In this phase, the peak ground acceleration (PGA) is systematically integrated into Newmark's displacement formula, enabling the incorporation of earthquake-induced landslides (EQIL). This formula is introduced in the last step of this chapter, and the determination of this seismic parameter will be discussed in detail in 11.4.4 Seismic Intensity: Subsequently, another integral component, the saturation ratio (m), is incorporated into the calculation of the factor of safety, also referenced in the flow chart in Figure 8. This ratio is adjusted based on specific hydrological conditions, facilitating a targeted examination of rainfall-induced landslides (RIL). The methodology used here, which relies on this adjustment, is explained in Section 11.4.5 Rainfall intensity,, which highlights the application of the method in assessing the influence of varying saturation levels on slope stability.

10.2.4 Calculating PGA Capacity with Fragility Curves:

PGA capacity is the capacity of a building or a bridge to withstand a certain level of PGA peak ground acceleration. With the help of fragility curves, we know how much damage a structure would incur at a given PGA. A structure's PGAcap (Peak Ground Acceleration Capacity) is the ground motion intensity level at which it has a 50% chance of reaching or surpassing a specific damage state. Usually shown as lognormal distributions, fragility curves illustrate the conditional probability of exceeding various damage levels given a particular amount of shaking. They are characterised by a median PGA (μ) and a dispersion (β). PGAcap is used to determine the point at which an asset is expected to sustain severe damage. It is computed as the median of the fragility function for a certain damage state. [3] For this thesis, the fragility curves for bridges were obtained from Moschonas et al. [11], and those for buildings were obtained from Rosti et al. [12]. This PGAcap was compared to the PGAdem, and if PGAcap > PGAdem, it means that the structure is safe during the seismic event and is represented by 1 in the scenario matrix. If the above statement is not true, then it is represented by 0 in the scenario matrix. It means that the building or bridge has sustained damage and is likely to disrupt the road network's functionality.

10.2.5 Factor of Safety:

Landslides in the Turin region, caused by earthquakes and/or rains, are often typified by shallow failure surfaces parallel to the slope surface. The rigid-block model is employed in this work. However, the infinite slope model with planar sliding surfaces and the limit equilibrium approach are frequently used to examine slopes of this type. It is recommended to use this model due to the deficiencies in understanding landslides that have previously occurred. Additionally, this is an excellent choice for the model that specifies the factor of safety because Newmark's technique, which employs the same rigid-block model, is widely used. In this situation, the rigid-block model is more suitable for assessing the possible displacements caused by seismic activity, as it assumes that the Earth's mass moves as a single, rigid unit. To determine the regions where EQILs or RILs may occur, the factor of safety can be computed using equation 7. FS can be expressed in various ways. The Jibson et al. equation is applied in this work:

$$FS = \frac{c'}{\Upsilon . t . sen\alpha} + \frac{tan\rho'}{tan\alpha} - \frac{m . \Upsilon\omega . tan\rho'}{\Upsilon tan\alpha}$$

Equation 1 factor of safety

c' represents the effective cohesion of the soil or rock material, which measures the internal bonding strength resisting shear forces. The unit weight of the material, γ, is the unit weight per unit volume and controls the forces of gravity on the slope. The thickness of the soil layer normal to the failure plane, t, controls the total weight and thus the forces driving the slope. The trigonometric functions sin(α) and tan(α) relate to the slope angle α, influencing the driving shear stress and the normal stress on the failure plane. The effective internal friction angle, ϕ', represents the strength of shear due to the forces of friction between the rock or soil particles. The parameter m represents the ratio of the saturated zone thickness to the total soil layer thickness, accounting for the effect of groundwater on slope stability. Finally, the volumetric weight of water is used to calculate the uplift forces in the saturated zone of the slope [41]. The equation is made so that the cohesive strength term is represented by the first term on the right-hand side, the frictional strength term by the second term, and the decrease in frictional strength as a result of soil saturation by the third term [42].

10.2.6 Critical Acceleration

Calculating the critical acceleration at which the slope will start deforming is the second step. Critical acceleration (a_c) is a crucial parameter when Newmark's displacement method is employed for assessing slope stability under seismic loading conditions. In fact, it acts as the point of break when the driving forces overcome the resisting forces and cause permanent displacement by defining the minimum value of horizontal acceleration to cause sliding on a slope. It is a product of the horizontal angle of the sliding block and the static factor of safety. According to Jibson et al., it is defined

$$ac = (FS - 1).g \cdot sin\alpha \quad (10\text{-}2)$$

Equation 8

g is the acceleration due to gravity, and FS is the determined factor of safety using Equation 7. The critical acceleration must be greater than zero to certify a slope as stable and resistant to ground motion without triggering a slide. The slope would be internally unstable if ac is negative, in all such situations, the slope is susceptible to a landslide merely because of its internal characteristics and gravity and not account of an external factor like earthquake or rainfall, A slope would be unstable if the safety factor calculated by Equation 7 is less than 1. Such slopes can collapse even without the influence of external factors such as earthquakes or heavy rainfall [32], [41].

10.2.7 Newmark's Displacement:

To apply Newmark's method, the Newmark displacement is calculated, resulting in a displacement value typically expressed in centimeters. It is important to note that this calculated displacement does not necessarily represent the actual effective displacement of the soil. Instead, it serves as an estimate of the potential movement of the slope under loading conditions, providing a measure of the slope's susceptibility to movement. DN is determined by the following expression [32] :

$$\ln(DN) = -1{,}708 + \ln\left[(1 - ac\ amax\ )\ 2{,}10\ (\ ac\ amax\ )\ -1{,}783\right] - 1{,}04 + (10\text{-}3)\ 30$$

Equation 9

The Newmark displacement is proportional to the critical acceleration, ac, as calculated in Equation 8, and the highest ground acceleration, amax. According to the formula, DN will only have a non-zero value if the ratio ac/amax is less than one, implying that ac is smaller than amax. So, for DN to be relevant, ac must be more than zero but less than amax; otherwise, DN will be zero, indicating no displacement. This condition ensures that the critical acceleration threshold is exceeded by the peak ground acceleration during seismic events, leading to slope displacement. [32]

10.2.8 Calculating the Efficiency Index:

The Efficiency Index of the road network is a way to quantify how the RN (road network) reacts to a natural hazard. It tells us how much the system will degrade or lose its efficiency after a natural hazard. In our case, the natural hazard is an earthquake. In this thesis, we use the Monte Carlo simulation to calculate the Em (mean efficiency of the road network). Specifically, after Nsim simulations of the seismic event, the post-event efficiency is assessed through Equation 4. Then, since a certain degree of uncertainty is considered in this study according to Equations 2 and 3, it is necessary to estimate the number of simulations after which the value of efficiency is stable (convergence analysis). To do this, the mean and standard deviation of the assessed efficiency index are evaluated as follows:

$$Em = \frac{\sum_{J=1}^{Nsim} Ep,j}{Nsim}$$

Equation 2

$$Estd = \left[\frac{\sum_{j=1}^{Nsim}(E,j - Ep,m)^2}{Nsim}\right]^{1/2}$$

Equation 3

where Ep,j is the maximum post-event efficiency among the roads that are still available, and Nsim is the total number of simulations. The values of Equation 10 and Equation 11 for Scenario Sc475 are depicted in Figure 8. This is for DS3; we did the same thing, but for all the other DS (Damage state) levels. I have attached all those figures in Annexure A. It is pertinent to mention that this Efficiency index is done for m=1, meaning the soil is fully saturated.

The mean efficiency index stabilizes after about 1500 simulations at approximately Em = 0.305. The maximum value of the pre-event efficiency ERNmax of the RN is 0.39. This means that, according to

our model, a seismic scenario with a return period of Tr = 475 years would result in an efficiency reduction of approximately 22% in the RN.

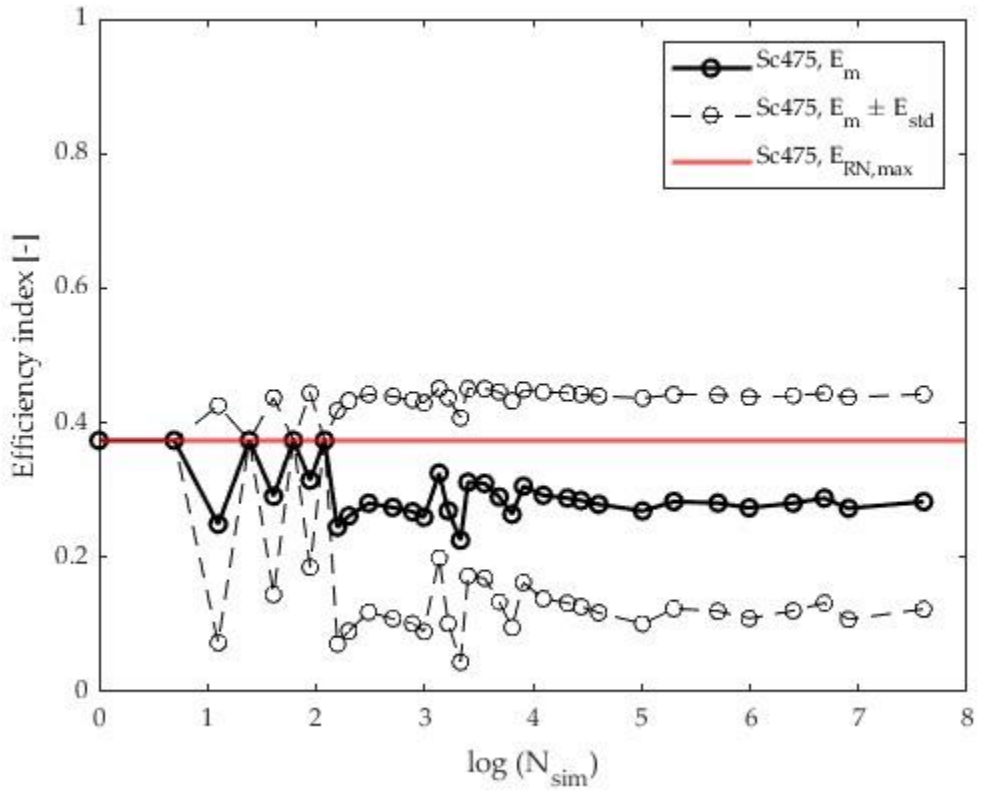

Figure 8 Application(Turin): Road network efficiency under a seismic scenario with return period T475 for DS3

10.3 Methodology for Estimating the cost of disturbances:

Calculating the cost associated with a hazard event is a challenging task, as numerous variables must be considered. The total cost can be divided into two broad categories: direct costs and indirect costs. The direct cost pertains to the cost of asset damage, the cost of human lives lost, and the unavailability of the road network [43]. This data can be taken from different post-hazard assessment reports. However, this still doesn't reveal the true cost, as most reports only indicate the physical cost of the hazard. They lack in calculating the social and environmental costs. This is especially true in mountainous areas, where a single road often connects most villages and towns. If these roads get damaged, not only are those communities cut off from the rest of the country, but local businesses alsoes get impact,eas touristssts or adventure seekers lose access to those sites. [44]. To calculate

10.3.1 Risk of Person

This direct impact on people due to natural hazard has three approaches we will consider the direct impact of the hazard event – standard situation (insert equation and table) was taken in terms of cars and number of people of traveling in the car, using the AADT (average annual daily traffic) we

assumed that each car carries 1.76 person. This way, we were able to assess how many people were affected.

$$r(DI)NS,j = pj \times (1 - pRb) \times (1 - pRbE) \times pN \times NP \times \lambda \times pSo,j \times fL$$

Equation 4 Direct impact of the hazard event – standard situation [15]

Table 2 Risk variables and their derivation for the calculation of RP: direct impact – standard situation [15]

Variable	Description	Derivation
r(DI)NS,j	Risk of person in scenario j (normal situation)	
pj	Probability of occurrence of an event (frequency of scenario J)	pj = fj − fj+1; fj = 1/Tj pj : probability of occurrence of scenario j fj : frequency of occurrence Tj : return period of scenario j
pRb	Probability of precautionary road blockage	
pRbE	Probability of road blockage due to event (road closure due to a previous event of the same hazard type along the road)	$PRbE = \alpha \times (1 - \frac{1}{nH})$ α: reduction factor1 event of the same hazard type along the nH: number of hazard areas with the same hazard road) process and triggering mechanism
pN	Probability of the standard (normal)	pN = 1 − pC situation
PC	Probability of a traffic jam (congestion)	$PC = (\frac{n}{365}) \times (\frac{D}{24})$ n: number of traffic jams per year D: average duration of a traffic jam in hours
Np	Number of affected persons	NP = NV × β NVN = MDT v×24 000 × l: number of vehicles in the standard situation NVJ = (ρmax×l) 1000 : number of vehicles in the case of a traffic jam MDT: mean daily traffic v: signalized velocity for cars in kilometers per hour (km h−1) l: length of the street segment in meters (m)3

		ρmax: maximum traffic density per lane and kilometre in the case of a traffic jam β: mean degree of passenger
ʎ	Lethality factor	Hazard-process- and intensity-related variable
pSo,j	Spatial occurrence probability of the process in the scenario j as proportion of the mean width or area of the process d domain in scenario j to the maximum width or area of the potential hazard scenario j domain	For rockfall processes $Pso,j = ET \times \frac{d}{Whd}$ ET: event type d: mean diameter of the block in metres (m) Ꮃhd = width or amplitude of the hazard domain in scenario j
f_l	Factors to differentiate the affected lane	0.5: one lane affected 1: whole road (both lanes) affected

10.3.2 Risk of Asset

Property risk refers to the potential for physical damage to infrastructure (e.g., buildings, bridges, roads themselves) due to natural hazards. The property risk due to the direct impact of the hazard process on the physical assets of the road infrastructure was calculated for each object i and scenario j using Equation 13, as shown in Table 3. The damage probability was assumed to be equal to the frequency of scenario j. The monetized costs refer to replacement costs and reconstruction costs, respectively.

$$r(DI)i,j = pj \times l \times Ai \times Vi,j \times pso,j \times fl$$

Equation 5 Calculation of Risk of Asset due to natural hazard [15]

Table 3 Risk variables and their description for the calculation of RA: direct impact. The calculation of the residual variables is according to Table 2

Variable	Description
r(DI)i,j	Risk of object i in scenario j in terms of a direct impact of the hazard
Ai	Asset value of object i
vi,j	Hazard-specific vulnerability of object i in scenario j
L	Length of affected road segment

10.3.3 Risk due to non-operational availability

The risk due to non-operational availability can be generally separated into economic losses due to (1) road closure after a hazard event or (2) because of precautionary measures for road blockage.

The former addresses the mandatory reconditioning of the road, and the interruption time depends on the severity of the damage. In our case study, this is associated with the closure of the road, resulting in a loss for local businesses and communities. Those who rely on this road for their daily commute and the transport of goods.

$$rRb,j = (pj \times fRB \times \frac{1}{nh}) \times DRb \times CRb$$

Equation 6 Risk variables

Table 4 . Risk variables and their description for the calculation of RD. The calculation of the residual variables is according to Table 2 [15]

Variable	Description
$R_{Rb,j}$	Risk of a roadblock in scenario j
fRb	Frequency of road blockage
DRb	Duration of road blockage depending on the hazard type in days (d)
CRb	Costs of road blockage in EUR
nh	Costs of road blockage in EUR

10.4 DATA SAMPLING:

To compute Newmark's displacement, all needed parameters must be precisely determined. Consequently, data sampling is a vital component of the case study. This procedure entails defining the required parameters at each stage or, if this is not possible, establishing acceptable estimates. While such simplifications are best avoided, they are occasionally inevitable. In some cases, values are awarded based on logical rationale and thorough explanation. This strategy is often necessary due to the impracticality of conducting examinations at each location separately in situ. The data sampling method includes measuring the slope angle, assigning soil properties to recognized landslides, analyzing seismic activity, and calculating rainfall intensity.

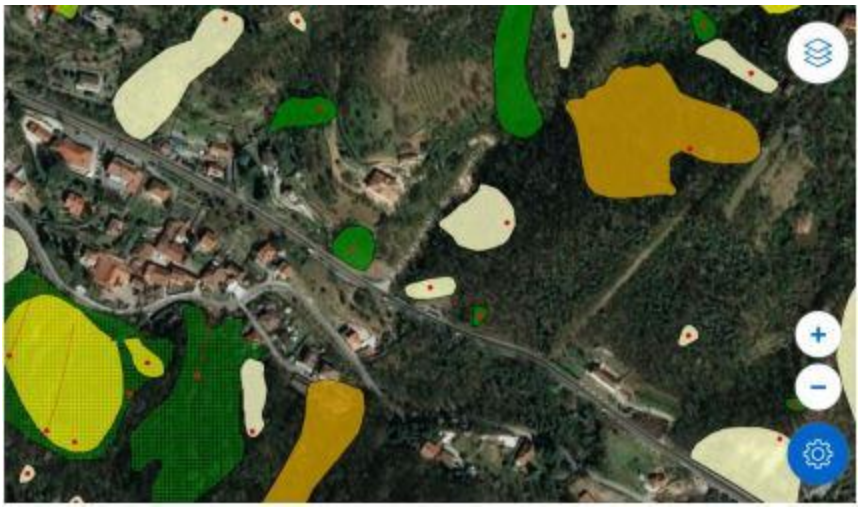

Figure 9 ISPRA-IdroGEO database visualising landslides LPN3, LPN4, LPN5, LPN6 and LPN7 [38]

The factors of safety, the critical acceleration, and Newmark's displacement were determined for every landslide that intersects or is near one of the 2 roads indicated in Figure 5. The ISPRA provides the area, location, and date of registration for each landslide – IdroGeo database (Figure 9). To allow individual study, each landslide is given a unique identity. The naming convention begins with the letter 'L', followed by the initial letter of the route where the landslide occurred and a sequential number, starting with one. Number one is the closest to Sassi. Figure 11 depicts, for example, landslides along the Pino Nuovo Road. The earliest landslide, closest to Sassi, is designated LPN1, while the latest, closest to Pino Torinese, is designated LPN13. Abbreviations for the roads are as follows: 'PN' stands for Pino Nuovo Road and 'PV' for Pino Vecchio Road. This systematic naming method allows each landslide to be uniquely recognized and analyzed.

Figure 10 Numbering of the landslides following the SS10

Each landslide was recorded in a GIS-based database, which is a critical tool for storing and presenting geotechnical information. This system enables the visualization of all pertinent data on a single platform, enhancing data analysis and understanding. Initially, an Online Street Map (OSM) served as the foundation layer, and the four selected roads, together with their respective start and finish locations, were added to the Geographic Information System (GIS). This created a clear visual depiction of the study area. The landslides of interest, especially those that cross or contact one of the four roadways as specified in the ISPRA-IdroGeo database, were then included in the GIS. This created a clear visual depiction of the study area. The landslides of interest, especially those that cross or contact one of the four roadways as specified in the ISPRA-IdroGeo database, were then included in the GIS. This integration provides a comprehensive and accessible method for studying landslides that impact the road network. By recording landslide data in a GIS-based database, the study employs advanced technical tools to efficiently store, display, and evaluate geotechnical data. This technique enables the visualization of spatial linkages and patterns in data, providing significant insights into the factors that influence the incidence of landslides and their impact on the road network. The use of GIS technology makes data more accessible and interpretable, facilitating the creation of effective risk reduction and infrastructure resilience measures.

10.4.1 Slope Angle:

The subsequent step in the methodology involves determining the slope angle, which is a crucial parameter for assessing landslide susceptibility. The specific position of each landslide was determined using Digital Elevation Models (DEM) and the previously built GIS database. This process enabled the extraction of elevation data for the top, bottom, and horizontal distance of each landslide. The elevation of the highest point (H1) and the lowest point (H2) was determined, enabling the calculation of the slope angle. The slope angle (α) was calculated using the following formula:

$$\alpha = \beta g \tan[(H2 - H1)lenghth]$$

Equation 7

For example, the slope angle of landslide LPN4 was calculated according to Figure 11. The exact location could be identified using the ISPRA database (Figure 10). Looking at the same place on the DEM, it was possible to determine the top and bottom heights of the slope, as well as the distance between them. It enables the accurate measurement of the angle of slope for each landslide by utilizing high-resolution elevation data provided by DEM. The use of DEM with the GIS database is not only useful for providing the precise calculation of slope angles but also enhances the total analytical power of the study. By systematically computing the slope angles, the study ensures that the crucial parameter is correctly represented, thereby enabling a more robust analysis of landslide dynamics and road network stability. Figure 11 is the DEM in which all the heights, bottom and top height, as well as horizontal lengths, are marked. This view provides the opportunity to explore all the slope angles quickly and effectively.

Figure 11 Representation of the heights and horizontal distance Lpn4

The next stage in the procedure is to assign all necessary soil properties. These metrics measure physical and mechanical qualities, including effective friction angle, cohesiveness, and volumetric weight. Using geological maps. These databases provide a reliable understanding of these factors.

10.4.2 Soil Parameters:

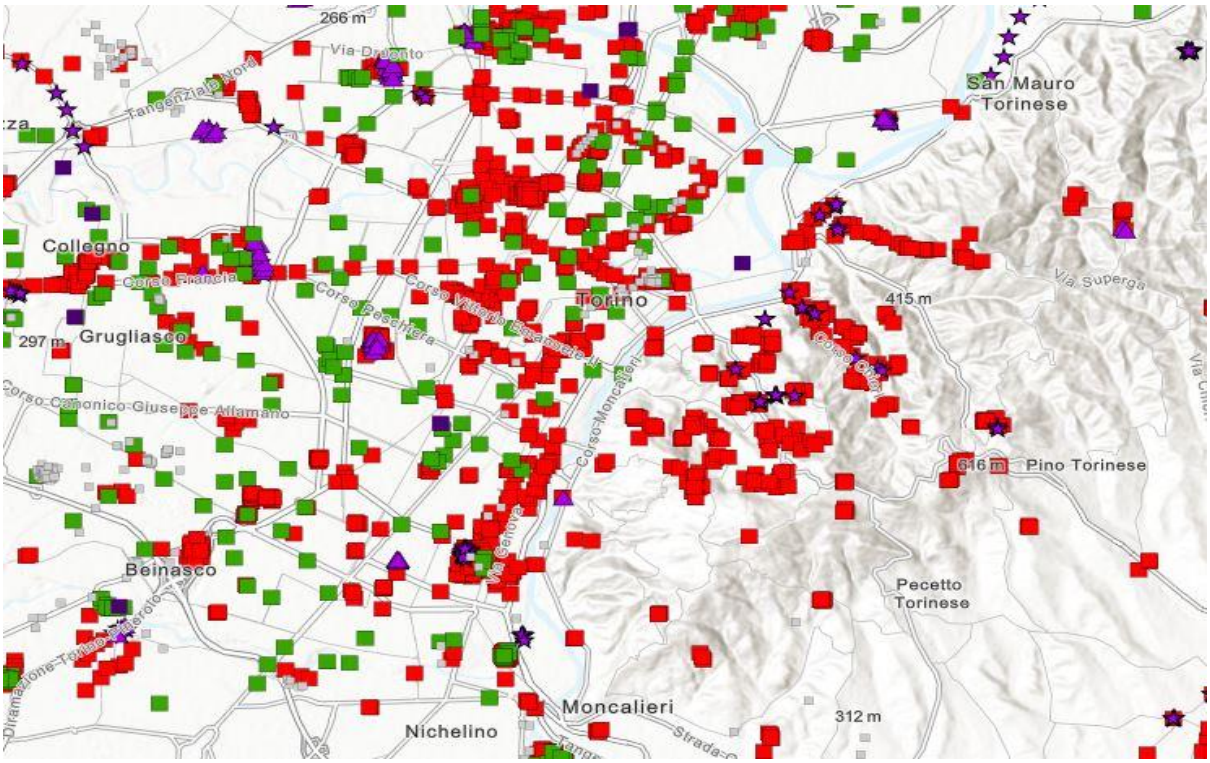

Figure 12 ARPA Piemonte database with red dots as survey points, green points as wells [45]

Samples from the ArcGIS web application, which were somewhat close to the research region, were uploaded to the project GIS, along with the corresponding perforations. This method makes it much easier to apply parameters to landslides. Furthermore, combining data from large-scale perforations

and small-scale sample analysis enables a thorough understanding of soil properties. This integration is essential for effective modelling and simulation in geotechnical engineering applications. Combining historical data with new results enables improved prediction of soil behavior under varied conditions, thereby increasing the reliability of geotechnical evaluations.

Nevertheless, it must be said that this method does not guarantee absolute certainty for these parameters, as perforations and samples were not always performed at the exact location of a recorded landslide. In situ testing should be conducted at specified places to ensure definite validation. These in situ tests are essential for obtaining accurate and site-specific data, which can then be used to verify the findings of the sampling and perforation analyses.

10.4.3 Building and Bridges data:

For this road network analysis, our scenario matrix also takes into consideration buildings and bridges along the road network that can potentially disturb the RN (road network) in case of an earthquake, Figure 13 depicts a scenario where a powerful earthquake can theoretically block the road which sits right in the middle of the valley. The road can be blocked by buildings collapsing on the road, or the bridge/ viaducts getting damage as well, to do this analysis it was important to get the data about all the buildings that line the road network, this data included the height of buildings, number of stories and the year they were constructed in. For simplification of calculations, it was assumed that all these buildings are constructed with masonry. Regarding the bridge and viaducts, it was essential to know the materials they were constructed from, the number of spans, and the type of bridge. In Table 1, the data regarding bridges and viaducts are shown.

This data was given to us by the Commune di Torino.

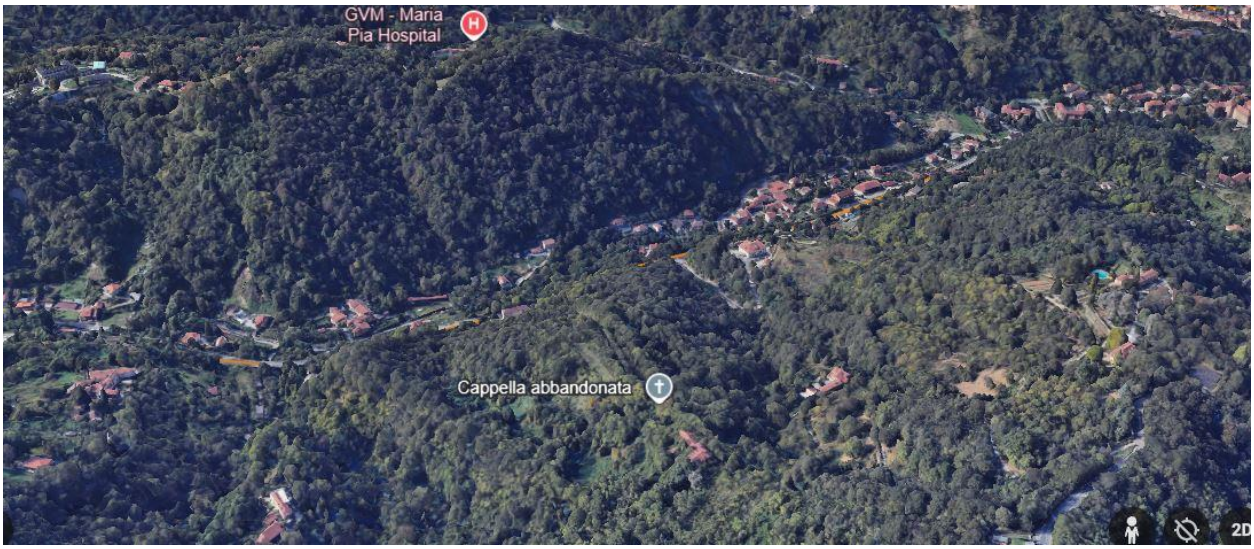

Figure 13 An area of potential road blockage due to landslide or building debris on the road, source Google Earth accessed 24th May 2025

10.4.4 Seismic Intensity:

In this study, the evaluation of landslide susceptibility considers not only the underlying geological and hydrological parameters but also crucial trigger variables, notably seismic impacts. To successfully incorporate seismic elements into landslide risk analysis, peak ground acceleration

(amax) has been used as a primary criterion. These figures are derived from a database maintained by the Istituto Nazionale di Geofisica e Vulcanologia (INGV), which provides a comprehensive seismic hazard model for the entire country of Italy. The approach for calculating the greatest horizontal acceleration caused by earthquakes requires the assumption of a specified seismic hazard probability. For this study, a probability threshold of 10% in 50 years was used to indicate the likelihood of an earthquake reaching the stated PGA value within the specified timeframe.

This probabilistic technique combines traditional seismic risk assessment practices with advanced methods to precisely determine the locations of the greatest seismic risk. The INGV database provides updated seismic hazard values for each 16 km^2 grid square, allowing for a more thorough and localized evaluation of seismic hazards. Given that the road network relevant to this project is contained inside a single such square, it is assumed that all landslides in this region are subject to the same maximum acceleration factor. This assumption enables the consistent use of seismic data in landslide susceptibility research, maintaining uniformity across the study area. Figure 14 depicts the squares with different PGA values surrounding Turin. The grid of interest is in Pino Torinese and can be seen in the bottom right corner of the picture. By incorporating these seismic factors, the study aims to enhance understanding of how seismic activity influences landslide occurrence and develop more accurate predictive models for landslide susceptibility in seismically active areas. The grid-based approach to the INGV database ensures that the analysis is based on strong, spatially resolved seismic hazard data, providing a solid foundation for estimating the risk of landslides triggered by seismic events.

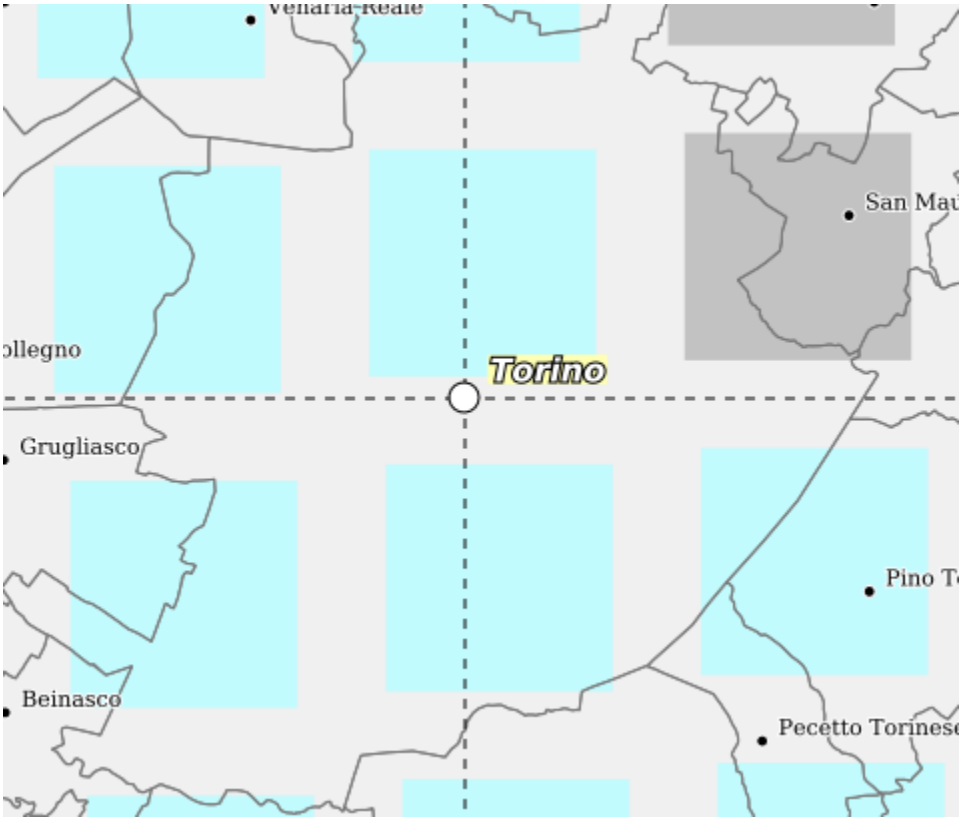

Figure 14 The grid-based approach to assigning PGA values in Turin [46]

The model used by INGV for calculating the peak ground acceleration values for Italy is MPS04. MPS04 (Modello di Pericolosità Sismica di riferimento del 2004) is a comprehensive seismic hazard model used for mapping and analyzing the seismic hazard in Italy, particularly in computing the Peak Ground Acceleration through the grid method. This model adheres to the principles of Probabilistic Seismic Hazard Analysis (PSHA) in estimating the probability of various levels of seismicity, employing a logic tree method to address natural uncertainties in seismic hazard calculations [47]. This model is essential for assessing seismic risks. It combines regional earthquake activity, the frequency of earthquakes, and the geological features of different areas to create a detailed seismic hazard map. PSHA is utilized in the MPS04 to compute the probability that certain levels of earthquake-induced ground motion will be exceeded at specific locations over a specified period. For MPS04, this analysis is essential in estimating PGA for different grid cells throughout Italy. It examines local earthquake activity, the frequency of earthquakes, and the geological characteristics of various areas to provide a comprehensive understanding of potential seismic impacts [47]. This method involves considering several possible models and assumptions at each decision point or node, including different seismic source zones, earthquake magnitude distributions, and Ground Motion Prediction Equations (GMPEs). Each option is represented by a branch in a logical tree and is assigned a weight that indicates its likelihood or believability, based on expert opinion and actual data. By this methodology, all possible outcomes and their corresponding probabilities are considered, providing a comprehensive assessment of seismic hazards. To effectively address the uncertainties associated with seismic hazard estimation, MPS04 utilizes a logic tree approach. It is a method in which different possible models and assumptions are systematically taken into consideration at every decision-making point or nodes like different seismic source zones, earthquake magnitude distributions, and Ground Motion Prediction Equations (GMPEs). [47]. Each option is represented by a branch in a logical tree and is assigned a weight that indicates its likelihood or believability, based on expert opinions or actual data. By using this method, all possible outcomes and their probabilities are considered, providing a detailed assessment of seismic hazards [48]. Central to determining PGA values across the grid in MPS04 is formula 10-5 for the probability of exceedance [49]:

$$\lambda_{IM>im^*} = \nu . P(IM > im^* | m, x, y)$$

Equation 8

λ (Lambda): This represents the annual rate at which a specific intensity measure (IM), such as PGA, exceeds a given threshold (im*) at a site.

• ν (Nu): The annual rate of earthquake occurrences affects the site.

• $P(IM > im* | m, x, y)$: The probability that the ground motion intensity exceeds the specified threshold given an earthquake of magnitude m occurring at location x,y. This probability is derived from selected and weighted GMPEs within the logic tree. The result is a set of probabilistic seismic hazard maps showing expected PGA values across Italy. Figure 15 is an example of such a hazard

map using MPS04 with a return period of 475 years. These maps represent the likelihood of exceeding certain ground motion levels within specified time frames, such as 50 years, and serve as essential tools for urban planning, 39 building codes, and seismic risk management. MPS04's comprehensive and probabilistic approach ensures that seismic risk maps are both scientifically robust and practically relevant, helping to improve safety and resilience in seismically active areas in Italy [47] [48],

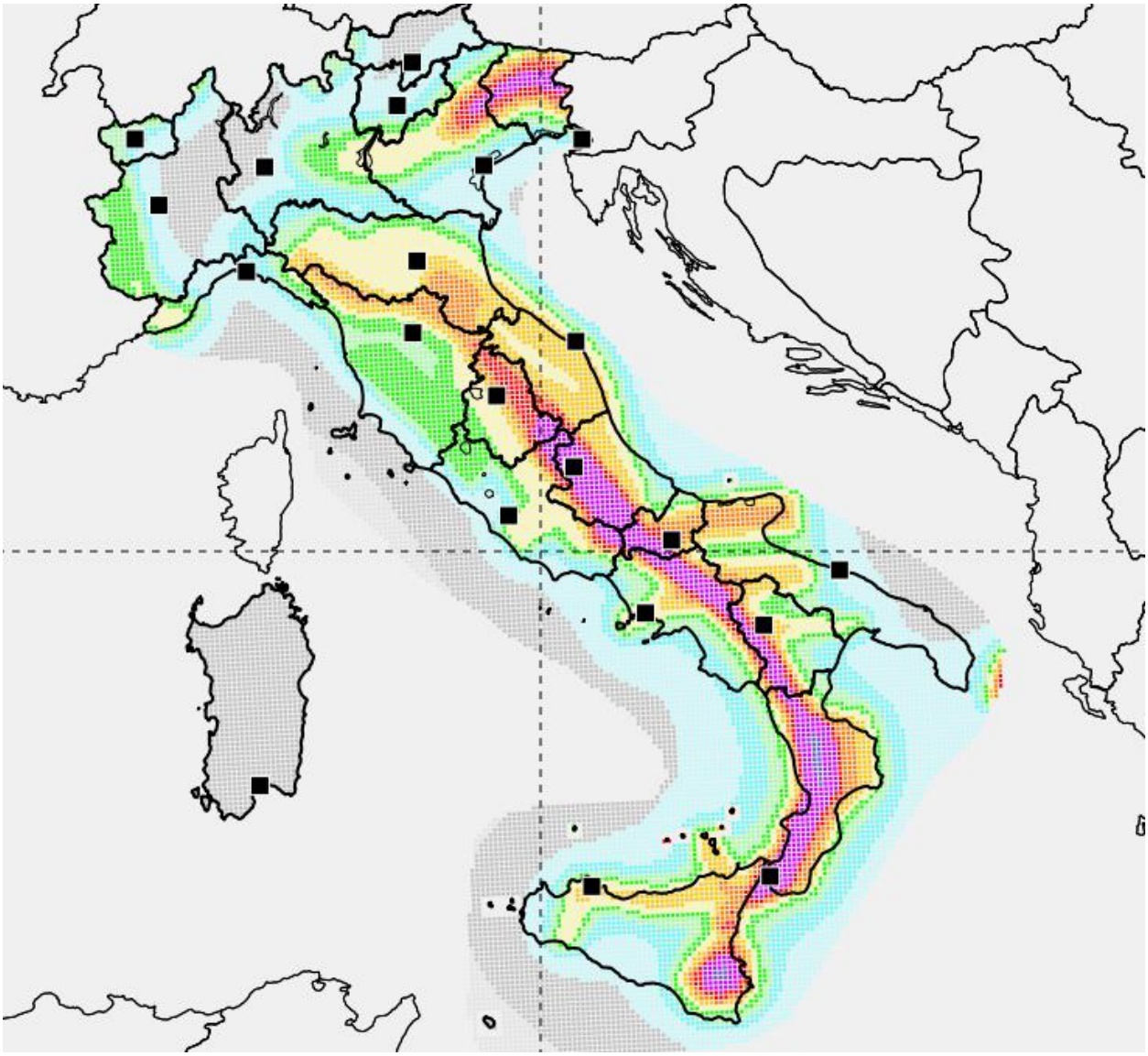

Figure 15 PGA hazard map of Italy using MPS04 [46]

10.4.5 Rainfall intensity:

In the current research, rainfall intensity is determined to be a fundamental trigger for landslide susceptibility, directly through its influence on soil saturation. This relationship is captured in the factor of safety (FS) equation, Equation 7 in this paper, where m is employed to symbolize the ratio

of saturated soil thickness to overall soil layer thickness. m appears in the numerator of a negative term in Equation 7. Thus, an increase in m, indicating greater soil saturation due to more intense rain, yields a larger negative value, hence reducing the overall factor of safety. Thus, a greater rainfall intensity, leading to greater saturation ratios, reduces slope stability and enhances failure probability. To accurately estimate the impact of rainfall on slope stability, assumptions regarding the value of m must be made. These assumptions are based on rainfall intensities anticipated or witnessed at respective levels of saturation, which have been calculated and documented by Meteoblue [50], a repository of all Piemonte rain over previous years. After arriving at these assumptions, additional computation can be carried out using the factor of safety already derived to calculate slope stability under different hydrological conditions. This systematic approach enhances understanding of the way rainfall integrates with geological conditions to affect landslide hazards, offering an integrated estimation of potential slope failure under various hydrological conditions.

10.5 Assumptions:

This chapter discusses the assumptions in the landslide hazard assessment project in more detail. In this study, it was frequently difficult to obtain the exact values of parameters for an in-depth analysis. This was usually due to limited site-specific information and practical constraints that deterred conducting extensive on-site tests within the locations of the observed landslides. The function of this chapter is to describe and defend the implicit assumptions of the research. In spite of the inadequacies of the material at hand, these assumptions were required to fill in the data gaps and enable the research to proceed. Through clearly outlining these assumptions, the chapter increases the transparency of the research methodology and enables consideration of how these assumptions impacted the findings of the study. It further identifies how crucial it is to know the assumptions behind evaluating the outcomes. This chapter also explains the rationale behind each assumption, so its need and grounds are clear. The assumptions are not simplifications in the sense that they are educated guesses and methodological choices made because the data were unavailable. They are needed to provide scientific rigor and methodological accuracy of the landslide hazard assessment so that conclusions reached are as valuable as the data permit. In effect, the assumptions discussed here are essential to construct the study framework and analysis method. They allow for continuation and finalization of the study by providing a systematic strategy towards proceeding with the analysis even in the absence of data. This makes sure that the end risk assessment is grounded in the best available scientific methods and data but is based on being dependent on some assumptions.

10.5.1 Infinite slope – Block failure:

The Limit Equilibrium Method (LEM) is used in this work under the assumption of a flat sliding surface, which streamlines the computation of the factor of safety. According to this assumption, linear equations based on the notion of translational equilibrium can be entered. These equations can be applied to a block that represents a localized failure (block failure) or to an elemental analysis typical of the potentially unstable parts of a slope (infinite slope model) [51].[AS1]

When the slope gradient is constant throughout its length and the soil thickness is substantially smaller than the slope's length, as shown in [52]Figure 16The infinite slope model is very suitable. A thorough examination of the ISPRA database's landslide data, however, reveals a variety of landslide

sizes, ranging from huge to quite tiny regions. Given that the lengths reported by ISPRA frequently reflect the whole region impacted by the landslide, including both the initial slide and later deposition zones, this variability calls for a rigorous assessment of the recorded data.

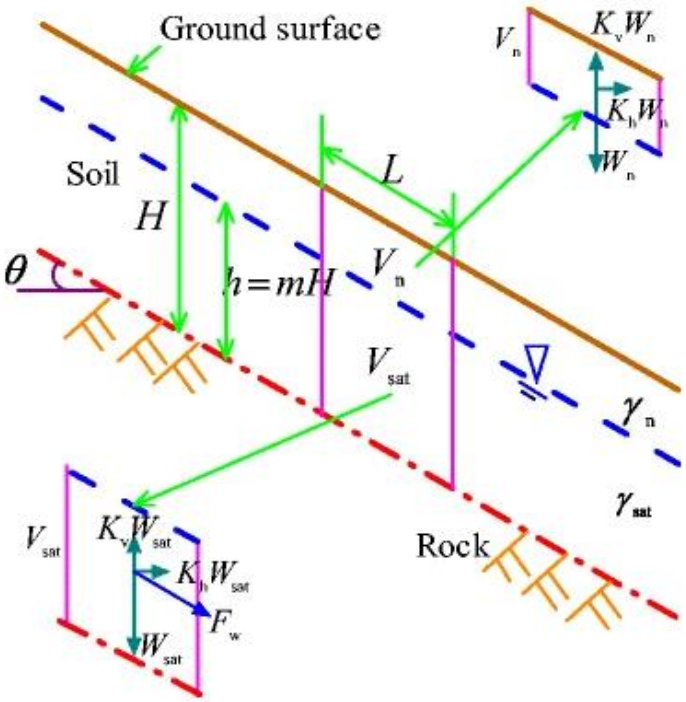

Figure 16 Geometry of the infinite slope surface [52]

When calculating the effective length of the slope for modelling purposes, for instance, the areas depicted in Figure 17 Include both the triggering zones and the deposition zones; the latter is a part of the landslide post-slide rather than the active sliding phase [52]. The applicability of an infinite slope model is called into doubt due to the tiny regions that were recorded, some of which had a total length (including deposition areas) of less than 20 meters. The viability of assuming an infinite slope under these circumstances is made more difficult by the fact that the depth of the sliding surface is still unknown and that there is no situ testing. Therefore, the infinite slope assumption must be removed due to the uncertainty in the length and depth of the sliding surfaces. Rather, the rigid-block model, which was first presented in the discussion of the factor of safety derivation Equation 1, is used in this work.

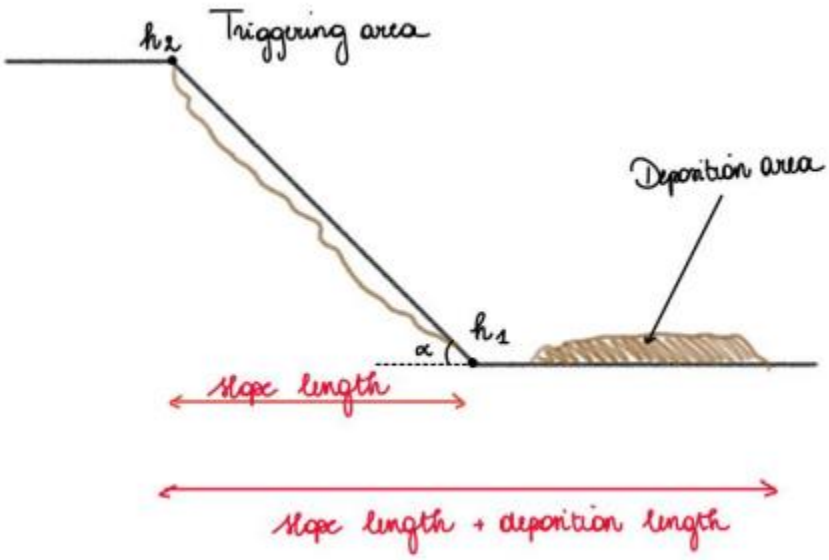

Figure 17 Representation of the effective slope length and the deposition area.

This model is supported by the need to address the translational equilibrium of a possibly unstable block inside the slope and is more appropriate for the circumstances and data restrictions found in the research region. The methodological framework employed in this study involves the adoption of a rigid-block model, which facilitates the application of Newmark's displacement calculations across the study region. This scientific approach ensures that the slope stability study will continue to be reliable and accurately represent the complex, dynamic conditions of the terrain. The method is designed to mitigate the inherent drawbacks resulting from the simplification required to accurately simulate such complex natural processes.

Nonetheless, the use of this method is based on several fundamental assumptions.

Below is a detailed description of the assumptions that underpin this research [51]

Plane Deformation Conditions: The study suggests that stability is unaffected by significant out-of-plane forces or deformations, and that deformation within the slope occurs in a plane, provided that plane deformation conditions are met. This assumption reduces the three-dimensional reality of slope behavior to a more manageable two-dimensional problem.

Uniform Factor of Safety: It is assumed that the factor of safety (FS) stays constant at all surface locations. Instead of specific variations that may arise from stress concentrations or heterogeneous material properties, this uniformity suggests that FS reflects a mean value, providing a generalized measure of stability throughout the entire slip surface.

Constitutive Law: Perfectly Plastic Rigid - The study employs the constitutive model of a rigid, completely plastic material. According to this rule, until the yield condition is satisfied, the rock or

soil acts as a rigid body; after that, it undergoes plastic deformation. Any strain hardening or softening that may occur in actual soil or rock masses is not considered by the model.

Sliding along a Presumed Surface: This approach assumes a predetermined, known (assumed) form for the slip surface. Throughout the study, this shape, which is usually reduced to a planar or curvilinear shape, is regarded as stable, and the soil or rock mass's sliding motion is limited to this surface.

10.5.2 Allocation of ground parameters:

Using soil samples collected from the ARPA Piemonte portal, the geotechnical parameters — such as the effective internal friction angle, effective cohesion, and volumetric weight of the soil— essential for determining landslide susceptibility were determined. Every sample gathered from the research region was meticulously entered into the project's Geographic Information System (GIS), and the parameters were allocated accordingly. These samplings were conducted on a smaller scale and did not encompass the entire road network due to its vastness. Due to this constraint, assumptions must be made to distribute these geotechnical factors among unsampled regions as accurately as possible. A spatial analysis method was employed within the GIS framework to address this issue. Each sampling location was surrounded by a buffer zone that was 500 meters in radius. Figure 18. The geotechnical parameters of the closest sample were applied to landslides that occurred within these buffer zones. The efficacy of the model is increased by doing this. By using this spatial analysis method, we ensured that the parameters are available throughout the entire road network. The average values of all the samples in the research region were computed to determine these default settings. It's also critical to remember that not every sample included full data for each of the three factors. Upon these situations, the respective landslides were assigned the available values from the samples, and any missing parameters were filled up with the previously stated default values. This hybrid technique enhances the accuracy of the assessment by ensuring that every landslide is evaluated using the most comprehensive data set available. The following are the computed default values:

- Effective cohesion (c'): 20.70 kPa
- Effective internal friction angle (ϕ'): 25.64 degrees
- Volumetric weight of the soil (γ): 19.19 kN/m^3

These values are tabulated (presented in Table 2And serve as a baseline for geotechnical characteristics in the broader study area, ensuring a consistent and systematic application of data in the landslide hazard assessment. By integrating both localized and averaged geotechnical data, this methodology not only compensates for the spatial variability in soil properties but also strengthens the predictive capability of the landslide susceptibility models developed in this research.

Table 5 Calculation of default values of the soil parameters.

Sample number	ϕ' [°]	c' [kPa]	γ [kN/m^3]
S1	25.70	24.60	/
S2	25.90	6.30	19.65
S3	23.30	17.70	20.87
S4	26.60	37.70	19.96

S5	26.10	31.70	18.97
S6	22.50	32.30	/
S7	28.60	26.70	20.00
S8	/	/	20.30
S9	/	/	17.50
S10	/	/	/
S11	/	/	18.30
S12	/	/	20.30
S13	/	/	17.80
S14	/	/	18.00
S15	/	/	20.32
S16	/	/	19.40
S17	/	/	17.28
S18	/	/	18.78
S19	/	/	18.35
S20	/	/	18.56
S21	24.90	9.70	18.02
S22	23.00	22.30	20.16
S23	23.70	17.70	19.80
S24	26.10	11.70	19.98
S25	31.30	10.00	19.91
Average	25.64	20.70	19.19

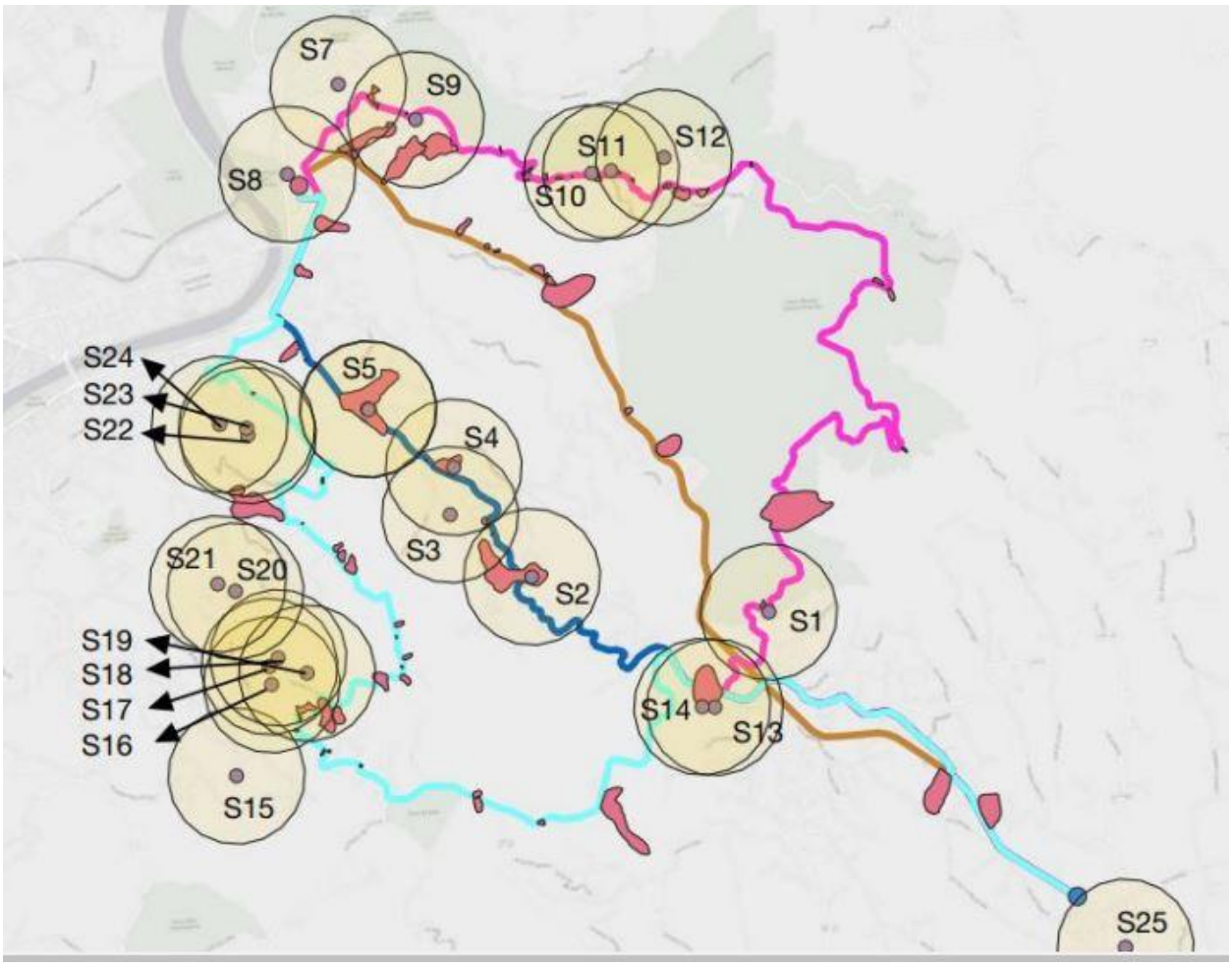

Figure 18 Project GIS with buffered samples (radius 500m).

10.5.3 Constants

The next chapter explains in detail two basic constants important to the geotechnical computations in this study. The constants are the weight of water, the volumetric and the gravitational acceleration. These parameters are well-known and do not require assumptions, simplifications, or solutions in various forms compared to other variables discussed in this study. Therefore, the values listed below are consistently used across all studies. Water's Volumetric Weight (γw): This constant is utilized when calculating hydrostatic pressure in soils. Its widely used definition is 9.81 kN/m^3 [52].Gravitational Acceleration (g): This constant, widely used as 9.81 m/s2, is utilized to calculate forces upon soil or rock masses [52].Given their critical importance in geotechnical calculations, these known values form the core of most analytical models used throughout this research, providing accuracy and consistency to all related analyses.

10.5.4 Soil thickness perpendicular to failure surface (t)

In this study, one of the most important assumptions is the soil thickness perpendicular to the failure surface; this variable is of critical importance but remains marked with considerable uncertainty. This is because soil is heterogeneous. In and around the Piemonte region, this is evident in the perforations undertaken by ARPA Piemonte. The variability in soil characteristics

makes it difficult for us to ascertain the soil thickness at any given point. This point is perfectly illustrated in Figures 18, Table 3, and Table 4. Due to its intricacy, it is often impossible to determine the crucial sliding surface solely from empirical data. Rather, the position of the possible sliding surface is estimated using predictive modelling, which helps determine the key factor of safety. This crucial factor of safety indicates the lowest stability point along the slope and is calculated at the expected depth of collapse. The pushing forces are most likely to outweigh the opposing forces and fail to achieve this crucial depth, as the soil's resistance is at its lowest. It should be noted that the safety factor may vary from this minimal value at depths other than the critical point. Still, it will always be greater, indicating less susceptibility to failure. A soil thickness assumption must be made due to the difficulties in modeling, forecasting, and precisely identifying this crucial failure surface through in-situ testing. A uniform depth of 3 meters is assumed for the soil thickness, based on recognized precedents in the field and consistent with approaches used in foundational publications by Jing et al. [53] and Xing et al. [52]. Because the boundary between two distinct soil layers is frequently one of the weakest points in the subsurface profile and may act as the critical failure surface, this depth is also a thickness that frequently recurs in the upper layer of the samples that were taken (Figure 18, [45] Table 3 & Table 4. It should be noted that while this 3 m number may be an accurate approximation in certain locations, it may also be quite close to reality in others. In the calculation for the factor of safety, a higher value for this depth below the surface will result in a lower cohesive strength component, which will lower this FS. As a result, slope stability will suffer from a higher value. As a result, slope stability will suffer from a higher value. A lesser depth, on the other hand, will benefit from higher cohesive resisting strains. For stability analysis under diverse soil conditions, this depth appears to be a suitable estimate, according to a synthesis of empirical research and literature. This assumption is crucial for advancing landslide susceptibility analysis, despite the inherent limitations of the available data and the practical constraints of in situ testing. By adopting this standard depth, the study aligns with established geotechnical practices, ensuring that the analysis remains robust and comparable with other studies in the field.

Table 6 Different layers of the ground in sample S15 [45]

Perforation Code	Depth (m)	Description
101771	3.00	Silt with sand
101771	6.00	Silt with sand interspersed with levels of small serpentinite nodules
101771	8.00	silt with fine sand
101771	14.10	fine sandy silt
101771	19.50	sandy silt, locally clayey with the presence of gravel and coarse sand
101771	19.90	pebbles and serpentinite strands
101771	25.00	medium coarse sand with silt and scattered serpentine pebbles
101771	26.40	silty sand
101771	29.00	Serpentinite is found in a sandy matrix

101771	30.00	sandstone with coarse gravelly and pebbly elements

Table 7 Different layers of the ground in sample S8 [45]

Perforation Code	Depth (m)	Description
2040	2.80	Fill material
2040	6.20	Fine weakly loamy sand
2040	8.50	conglomerate with little sand and clay
2040	15.10	conglomerate and medium fine sand
2040	19.60	Clayey sand passing through very fine compact marl

10.5.5 Saturated thickness compared to the total layer thickness (m)

10.5.6 Travel Time and Traffic Demand:

10.6 Calculations

A thorough review of the computer methods used for landslip sensitivity analysis is included in the next portion of this thesis. The application of theoretical models and presumptions discussed in earlier chapters is demonstrated using a concrete case, which is essential to this discussion.

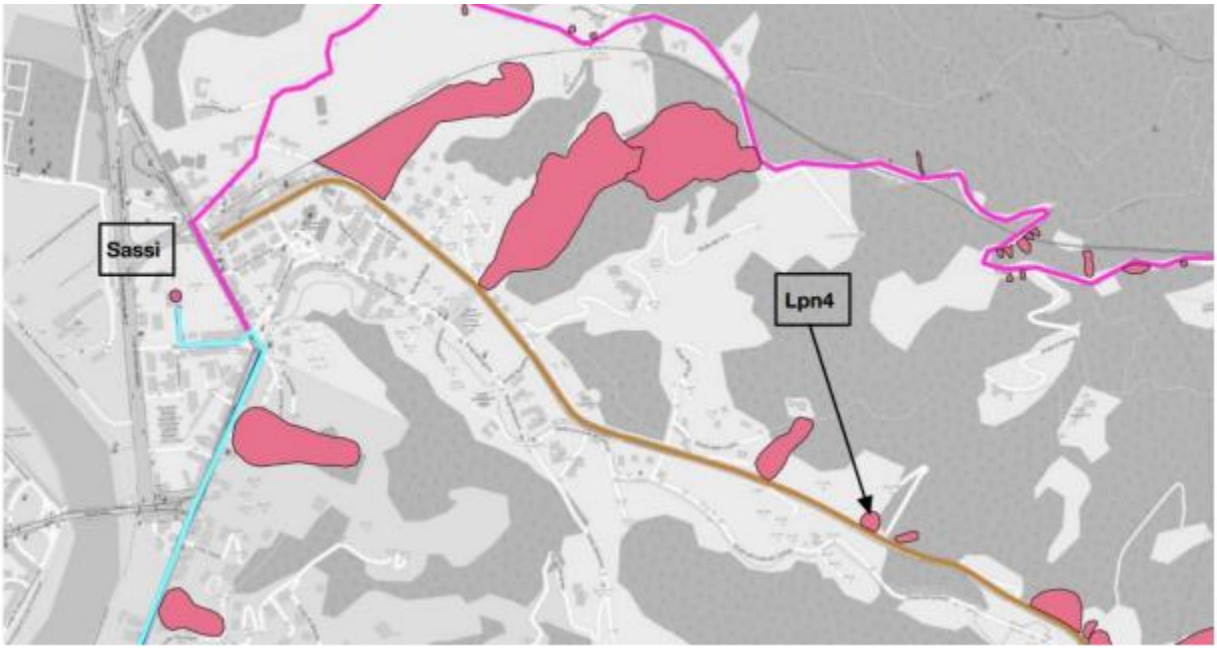

Figure 20 Localization of landslide LPN4.

Landslide LPN4 was chosen as a sample case study for this reason. Figure 20: Landslide LPN4 Localizations. According to the ISPRA database, landslide LPN4 is located along the Pino Nuovo (SS10) road, which begins at Sassi. Due to its location and the traits it shares with previous landslides in the area, this specific landslide —the fourth in a series from Sassi —is a relevant example. The selection of LPN4 permits an in-depth exploration of computation procedures, enabling a step-by-step illustration of how environmental conditions, theoretical assumptions, and geotechnical

properties are integrated to predict stability and evaluate risk. Besides describing the unique dynamics of LPN4, this study will offer a model for extrapolating the general implications of the findings to comparable landslides within the study area. The subsequent calculations will closely adhere to the step-by-step method outlined in the previous sections, ensuring that every stage is unambiguous and reproducible, from the initial sets of parameters based on presumptive conditions to the ultimate evaluation of landslip susceptibility.

10.6.1 DS Values:

We calculated the DS values of our bridges and buildings using the methods of Moschonas et al. [11] and Rosti et al. [12], respectively. All the bridges in our road network (RN) are of the same type, characterized by a Bridge with a slab (solid or with voids) deck, monolithically connected to multi-column bents, as described in code 311 by by Moschonas et al. The Siatista bridge's graph B (Transverse Direction) was used to calculate the actual values. The Moschonas paper employed the pushover analysis technique to generate the pushover curve, and the damage state was assessed primarily in terms of parameters from the pushover curves of generic bridges, along with local quantities such as bearing deformation. The fragility curve presented is one of the comprehensive fragility curves set in Europe.

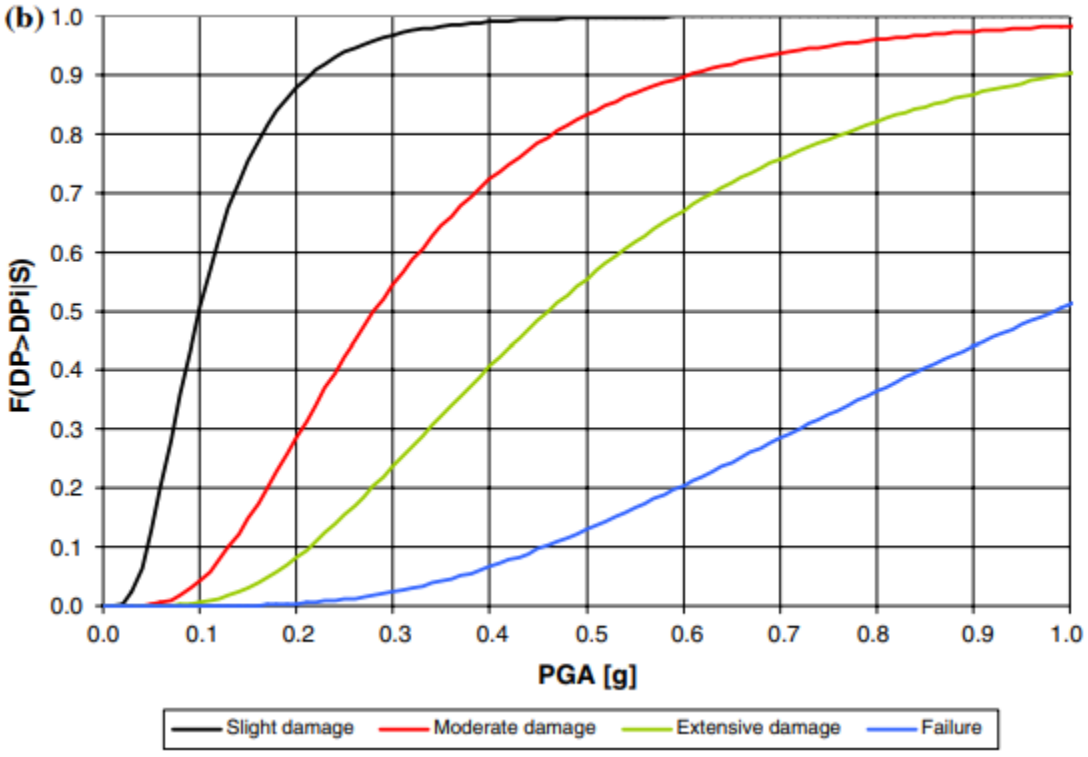

Figure 21 Fragility curves of the Siatista bridge. [11]

10.6.2 Calculation of the slope angle

These parameters, identified as H1, H2, and the horizontal length, are essential in calculating the slope angle with precision. In this instance, as depicted in Figure 11, landslide LPN4's parameters have been established and measured: H1, the elevation of the landslide base, is at 285,00 meters

above sea level. In contrast, H2, the peak elevation, stands at 307,00 meters. The shortest horizontal distance between the two points is measured as 35,07 meters. These are utilized in Equation 15 as follows

$\alpha = Bgtan$ [307m − 285m 35,07m]

Equation 17

The resultant angle (α), in Equation 17, is 32,10 degrees, corresponding to about 0.56 radians. The following data indicate the steepness of the slope and are vital in the analysis seeking to test stability and estimate the potential susceptibility of the terrain to landslide events. The calculated slope angle will be used directly in the next step of the analysis, calculating the factor of safety.

10.6.3 Calculation of the factor of safety

The safety factor (FS) depends on several variables that affect slope stability. To account for the variety in soil moisture levels, two scenarios are considered: totally dry soil and fully saturated soil. The parameter m, which denotes the ratio of saturated thickness to total layer thickness, is set to zero in the case of dry circumstances as explained in the last chapter. This suggests that there is no saturation, and because there is no pore water pressure, the soil is thought to have its maximum shear strength. Conversely, in the fully saturated scenario, m is set to one, indicating complete saturation where the entire soil layer contributes to potential sliding, drastically reducing the cohesion strength and internal friction. For both scenarios, the remaining parameters such as the effective friction angle, the effective cohesion, and the volumetric weight of the soil are held constant. These parameters are derived from data integrated into the project's Geographic Information System (GIS), which includes relevant soil samples obtained from ARPA Piemonte. As instructed in the assumptions of this study, any landslide occurring within a 500-meter radius of a sampling 52 point inherits the geotechnical properties of that sample. However, it is noted in Figure 20 that landslide LPN4 falls outside any defined sample buffer zones. Consequently, this landslide must be assigned the default values as calculated and tabulated in Table 5. Additionally, two constant values that are critical to the FS calculation include the volumetric weight of water and the assumed depth of the sliding surface, parameters that are predefined based on literature and empirical studies. The slope angle, previously determined through trigonometric calculation, also plays a crucial role in the safety factor computation. The parameters utilized in the calculations, along with their respective values, are listed below:

- Effective friction angle (ϕ’): 25,64° → 0,45 rad
- Effective cohesion (c’): 20,7 kPa • Volumetric weight of the soil (γ): 19,19 kN/m^3
- Volumetric weight of water (γw): 9,81 kN/m^3
- Slope angle (α): 0,56 rad
- Saturated thickness compared to total layer thickness (m): 0 – 1
- Soil thickness perpendicular to failure surface (t): 3m

Examining the first case in which m equals zero and putting these values into Equation 7, it is noticed that the last phrase of the formula no longer contributes to the value of FS owing to the factor of zero. The following describes how these values are applied within the formula:

$$FS = \frac{20.7\ kPa}{19.19\frac{kN}{m^3}.3m.\sin(0.56)} + \frac{\tan 0.45}{\tan 0.56} - 0$$

Equation 9 factor of safety calculation m=0

The answer to Equation 18 is 1.44. This computed factor of safety indicates the slope's stability under presumptive dry conditions. A slope that has a factor of safety of more than one suggests that it is stable in the present and has enough resistance to prevent possible sliding.

In the second scenario, where m is set to one to represent fully saturated soil conditions, these values are incorporated into formula 10-1. Under this assumption, the effect of water saturation on soil stability is maximized, directly impacting the calculation of the safety factor. Unlike the first scenario, the last term of the formula, which accounts for the impact of saturated soil, becomes a significant contributor to the overall calculation. The application of these values within the formula is detailed as follows:

$$FS = \frac{20.7kPa}{\frac{19.19kN}{m^3} \times 3m \times \sin(0.56)} + \frac{\tan(0.45)}{\tan(0.56)} - \frac{1 \times 9.81kN/m^3 \tan(0.45)}{19.19\tan(0.56)}$$

Equation 10 factor of Safety Calculation m=1

The factor of safety calculated under fully saturated conditions yields a value of 1,05, as derived from Equation 19. This value indicates the stability of the slope when subjected to maximum water saturation. A factor of safety greater than 1 suggests that, despite the adverse conditions assumed in this scenario, the slope maintains enough resistance against potential sliding. Relative to the first scenario, the factor of safety will invariably be greater because the removal of this negative term ensures that the reduction in cohesive strength caused by higher saturation is mitigated.

10.6.4 Critical acceleration

The determination of the critical acceleration, ac, is conducted using the safety factors derived under the two specific conditions: a completely dry scenario and a fully saturated scenario. The critical acceleration is calculated with Equation 8, where g is the acceleration due to gravity, FS is the factor of safety under static conditions, and α is the slope angle. For the scenario where m = 0, indicating a completely dry condition, the calculation is done in the following equation:

$$ac = (1.44 - 1)g \times Sin(0.56)$$

Equation 11 critical acceleration for m=0

Given these conditions, the previously determined factor of safety indicates that the slope is stable and exhibits a more robust resistance to seismic activity, as the critical acceleration required to

initiate sliding is large, equivalent to 0.23g, as calculated using Equation 20. The following equation is used to do the computation for the case where m = 1, which indicates fully saturated conditions:

$$ac = (1{,}05 - 1)g \times \sin(0.56)$$

Equation 12 critical acceleration for m=1

On the other hand, the factor of safety is reduced when m equals one, which denotes a fully saturated state, because water saturation significantly reduces soil strength. According to Equation 21, this condition implies a lower critical acceleration of 0.027 g, which means that even smaller seismic forces may cause slope failure. This indicates a higher danger of landslides in saturated circumstances, which is especially important when evaluating how the slope will behave during intense rainstorms.

10.6.5 Newmark's displacement

By setting m to one, rainfall is regarded as the only triggering element in this analysis phase, replicating totally saturated soil conditions. This configuration facilitates the assessment of the slope's stability under hydrological loads alone, excluding seismic forces. The next phase in the research involves determining Newmark's displacement, which adds seismic triggers to the computation. This displacement integrates the peak ground acceleration associated with earthquakes and measures the potential movement of the slope caused by seismic activity.

First, the example will consider only earthquake-induced landslides (EQIL), evaluating the slope's vulnerability to seismic triggers. By separating the consequences of seismic activity, this method makes it evident how it directly affects slope stability. Following this, the analysis will expand to incorporate both hydrological and seismic triggers in the second scenario, which considers fully saturated conditions. This approach acknowledges the interplay between these two critical factors. The calculation of the peak ground acceleration is done by using the INGV database. There is a 10% probability over 50 years, as described in the assumptions, and the following table is computed. With these conditions, the annual frequency of exceedance amounts to 0,0021. It means that the PGA in the 50th percentile is equal to 0,050g, as shown in Table 8

Table 8 PGA value for annual frequency of exceedance [46]

Acceleration values for Annual Frequency of Exceedance (point coordinates: Lat. 45.048 Lon.7.760 id13794)			
	PGA (g)		
Annual frequency of Exceedance	16th Percentile	50th Percentile	84th Percentile
0.004	0.0442	0.0709	0.0884
0.001	0.0341	0.0585	0.0713
0.0021	0.0271	0.05	0.0591
0.005	0.019	0.0399	0.0469
0.0071	0.0162	0.0364	0.0418

0.0099	0.0138	0.0332	0.0378
0.0139	0.0112	0.0299	0.0341
0.0199	0.0084	0.0263	0.0302
0.0332	0	0.0213	0.0246

It is assumed that the Peak Ground Acceleration (PGA) value of 0.050g is constant throughout the entire area, including the road network. To determine Newmark's displacement for landslide LPN4, this PGA value will be used. The following is how DN is calculated in situations with completely dry soils:

$$\ln(Dn) = -1.708 + \ln\left[\left(1 - \frac{0.23g}{0.050g}\right)^{2.10} \left(\frac{0.23g}{0.050g}\right)^{-1.783}\right.$$

Equation 13 ln(Dn)

The equation's critical acceleration is greater than the maximum acceleration. The Newmark's displacement cannot be computed and is assumed to be zero when ac divided by amax is greater than one, as was covered in section 11.2.7 Displacement analysis. Also, Equation 22 shows that an outcome is not possible because a negative term is raised to the power of 2,10

In the second scenario, in fully saturated conditions, the calculation of DN is outlined below:

$$\ln(Dn) = -1.708 + \ln\left[\left(1 - \frac{0.027g}{0.050g}\right)^{2.10} \left(\frac{0.027g}{0.050g}\right)^{-1.783}\right.$$

Equation 14 ln (Dn)

In Equation 23, there is a Newmark's displacement because the critical acceleration is lower than the maximum acceleration. The displacement, DN, that results from the logarithmic transformation is determined to be 0.11 cm. It is important to note that this figure does not definitively predict that the ground will be displaced by exactly 1.1 mm. Rather, this value serves as an indicator of the potential impact of seismic activity on the slope's stability.

10.6.6 Peak Ground Acceleration:

To understand if our building & bridge are damaged due to the seismic event, we must calculate the PGA capacity. We must calculate the PGA capacity for each DS level. Calculating the DS values has been discussed in the previous chapter. Since we have 5 DS levels, and for each path, we have numerous buildings, we calculate the the PGA capacity value for every building. And then compare that to the PGAdem. Below in Table 9, you can see the first 10 PGA values for each DS level; there are more than 300 buildings in each path. After this, we compare these values to the PGA cap. If PGAcap > PGAdem, then the matrix registers a zero value, which means no damage; otherwise, the Matrix will register a value of 1, which means damage, and the RN will be disturbed.

Table 9 First 10 PGA values for each DS level for Path 2

DS1	DS2	DS3	DS4	DS5
2.03368	0.307496	0.120814	0.250749	0.88226

3.700816	0.787685	2.167996	0.161458	0.70314
1.893323	0.248151	2.311677	0.32242	11.50475
0.702762	0.793322	0.260851	0.202837	0.461686
0.821124	0.185659	0.512907	3.863288	0.227081
0.268324	3.809199	0.954048	6.142788	6.332601
0.247239	3.278477	0.114399	5.621613	5.022014
0.201798	1.403366	0.723094	0.786116	10.94464
0.728268	0.40586	2.904128	0.83226	5.927901
0.426631	0.53597	1.413407	6.259996	9.422686

11. Discussion of results:

To do a comprehensive discussion on the multi-hazard analysis of our road network. We will discuss the data as tabulated in the appendices. This discussion will precede an evaluation of Newmark's displacement results, providing a comprehensive view of the study's findings on slope stability in various scenarios and conditions. The tables provided in Appendix A detail the FS and ac values for Pino Nuovo Road (SS10) and Pino Vecchio Road under both saturated (m = 1) and dry (m = 0) soil conditions. Each table presents the variability in slope angles, corresponding safety factors, and accelerations, reflecting the dynamic and complex nature of the terrains under study. The tabulated results in the appendices explicitly highlight instances where the factor of safety values fall below one, which are specifically marked in red to denote critical conditions. Each instance of an FS value is less than one associated with a negative value for critical acceleration. This suggests that no additional external triggers are required to initiate substantial horizontal displacement, which could lead to slope failure. Under such conditions, the slopes are inherently unstable and could fail under their natural circumstances. Appendix B details the results of Newmark's displacement calculations for each landslide across the four roads. Landslides with a factor of safety below one, leading to a negative critical acceleration, are denoted in red. According to the calculations, these landslides are predicted to experience no displacement. However, this is likely an oversimplification, as such slopes are inherently unstable. Displacement is probable even in the absence of seismic activity, and any seismic events would only exacerbate this instability.

Additionally, certain landslides are highlighted in yellow, indicating a calculable displacement value (DN). These landslides display an FS marginally above one, resulting in a low critical acceleration. This low threshold suggests that even minimal seismic activity has the potential to induce failure and plastic deformation of these slopes. This information is crucial for the risk assessment and management of such landslide-prone areas, highlighting the need for watchful monitoring and preventive strategies to effectively address potential slope failures. Examining the characteristics of the landslides in detail gives a better understanding of their behaviour. The analysis shows that most landslides happen on steeper slopes. Except for LPV9 and LPV11, which have slopes of 27.6° and 27.0°, respectively, all failures, encompassing both earthquake-induced landslides (EQILs) and rainfall-induced landslides (RILs), occur on slopes with inclinations exceeding 30°. These exceptions are characterized by notably inferior soil properties, specifically lower effective cohesion (c'). A critical aspect of the findings is the stark contrast between the outcomes under the best and worst-

case scenarios. As anticipated, the likelihood of failure under fully saturated conditions is substantially higher compared to dry conditions. In Appendix C, the DS values for all the bridges are given; similarly, we have calculated the DS values for the buildings as well. As discussed, we have used these DS values to calculate the PGAdem and compared it with PGAcap. In Appendix D, we have the results for the efficiency index. Keep in mind that these results are for m=1 and can be done again for m=0. The reason for m=1 is that this is the worst scenario we can have.

Figure 22 shows the efficiency index for DS1, indicating that the mean efficiency index stabilizes after approximately 2000 simulations at Em = 0.168. The maximum value of the pre-event efficiency ERNmax of the RN is 0.39. This means that, according to our model, a seismic scenario with a return period of Tr = 475 years would result in an efficiency reduction of approximately 57% in the RN. Figure 23 shows the result for DS2, where the mean efficiency index stabilizes after 2000 simulations at approximately Em = 0.19. The maximum value of the pre-event efficiency ERNmax of the RN is 0.39. The total efficiency drop in this case is 48%. The situation with the DS3 has been previously discussed, and the efficiency drop is 22%. For DS4 and DS5, the efficiency drop is 8%. The reason for the efficiency drop is that as we increase the DS level, the threshold for accepted damage also increases. This means that an 8% efficiency drop for DS level 4 is more dangerous than a 22% drop for DS level 3. In the next step, we have tried to calculate the cost of this efficiency drop for DS3. The total annual loss for a 22% efficiency drop is €30449409976.88 ± 14865732600.62

12. Conclusion

This thesis addressed the central challenge of ascertaining road network resilience in the case of a range of natural hazards. Recognizing an important gap between the analysis of singular structures and the actual functioning of a complete network, this study established and successfully evaluated an integrated, multi-level method. The key contribution of this work is that site-specific, detailed geotechnical hazards, such as landslides, can be correlated with their broader impact on general network transportation efficiency, particularly in emergencies. At the center of this research was a pioneering two-stage methodology. At the macro level, we formulated a method to quantify road network efficiency based on travel time to critical facilities, i.e., hospitals. This method encompasses various classes of disturbances, from direct structural disturbances, such as the collapse of bridges, to roadblocks that indirectly affect. At the micro level, we conducted a comprehensive geotechnical assessment to quantify one of the major dangers: slope instability. Through the integration of seismic data (PGA), soil saturation parameters, and Newmark's displacement, we developed a predictive model for landslide hazard on major road corridors, eliminating the need for complicated hydrological data. The application of this hybrid framework to case studies surrounding Turin, Italy, yielded valuable insights. Network-level analysis highlighted the vulnerability of connections to critical services following the event, quantifying the importance of maintaining routes open for emergency response. The extensive geotechnical study revealed that slope instability in the area in question was much more sensitive to saturation caused by heavy rainfall than to direct seismic initiators. Several slopes were discovered to be naturally unstable under saturated conditions (FS < 1) even without an earthquake, which also emphasizes the need for a multi-hazard approach. With the incorporation of these landslide forecasts into the network model, this research demonstrates how local geotechnical failures can induce cascading effects,

significantly compromising the overall efficiency of the transportation system. Ultimately, this thesis offers a completer and more practical tool for engineers, planners, and disaster managers. It merges structural and transportation engineering with a broader perspective on true systemic risk. This is a worthwhile contribution that offers valuable insights into studying and enhancing the safety of road infrastructure, enabling the identification of high-risk areas and targeted interventions accordingly. By observing how cumulative steep slopes, soil properties, and rain all act to destabilize a network of hillslopes, stakeholders are in a better position to design effective and targeted mitigation strategies. Future research may draw on this foundation. The model proposed here is highly adaptable and could be further developed by incorporating other non-seismic and seismic hazards, such as rain-driven flooding or earthquake-triggered landslides, under different geological conditions. Additionally, cross-validating the model across different geographical locations, such as flood-prone areas or other critical infrastructure sites like road tunnels, would further enhance its relevance. These efforts will continue to yield more powerful and resilient transportation systems that can withstand the challenges of future complexities. In the future, this research can be used to assess more deeply the impact on local communities. Also, what measures can we take to make our infrastructure more resilient to always ever-changing natural hazards?

13. Bibliography

1. Guha-Sapir, Debarati e I. S. a. A. Borde., The economic Impact of natural disaster, Oxford University Press, 2013.

2. L. Sorrentino e L. Giresini, «Risk assessment of road blockage after earthquakes,» *Buildings,* vol. 14, n. 4, p. 984, 2024.

3. A. Miano, M. Civera, F. Aloschi, V. De Biagi, B. Chiaia, F. Parisi e A. Prota, «Efficiency Assessment of Urban Road Networks Connecting Critical Node Pairs under Seismic Hazard,» *Sustainability,* vol. 16, n. 17, 2024.

4. P. Rodger, A cura di«Scots road plagued by landslides shut one day per week over four years causing ‘misery for motorists’,» 23 Nov 2024.

5. «What is a landslide and what causes one? | U.S. Geological Survey».

6. B. S. ,. D. P. D. P. C. H. a. J. S. Mike G Winter, «The Economic Impact of Landslides and Floods on the Road Network,» *Science Direct,* vol. 143, pp. 1425-1434, 2016.

7. S. O. Ben, «Significance of Road Infrastructure on Economic Sustainability,» *American International Journal of Multidisciplinary Scientific Research,* vol. 5.4, pp. 1-9, 2019.

8. B. M. a. N. M. Wassmer, «Resilience of transportation infrastructure networks to road failures Special Collection: Nonlinear dynamics, synchronization and networks,» *Chaos,* vol. 34, p. 13124, 2024.

9. S. Y. E. a. A.Erdem, «Monetary risk assessment for road networks exposed to seismic hazard in Istanbul,» *Natural Hazards,* vol. 119, pp. 445-466, 2024.

10. S. A. M. M. G. W. a. A. M. K. S. A. Argyroudis, «Fragility of transport assets exposed to multiple hazards: State-of-the-art review toward infrastructural resilience Highway and roadway infrastructure Numerical modelling Earthquakes Landslides Liquefaction Flooding Scouring Multiple hazardsLandslides,» *Singap World Sci,* 2019.

11. A. J. K. P. P. V. P. T. M. a. P. T. I. F. Moschonas, «Seismic fragility curves for Greek bridges: Methodology and case studies,» *Bulletin of Earthquake Engineering,* vol. 7, n. 2, pp. 439-468, 2009.

12. A. D. G. C. R. M. e. a. Rosti, «Empirical fragility curves for Italian residential RC buildings.,» *Bull Earthquake Eng,* vol. 19, pp. 3165-3183, 2021.

13. Y. Wu, G. Hou e S. Chen, «Post-earthquake resilience assessment and long-term restoration prioritization of transportation network,» *Reliab.Eng.Syst,* p. 211, 2021.

14. H. X. L. J. Yin, «Measuring the structural vulnerability of road network: A network efficiency perspective.,» *Shanghai Jiaotong Univ. (Sci.,* vol. 15, pp. 736-742, 2010.

15. P. S. S. F. Stefan Oberndorfer, «Multi-hazard risk assessment for roads: probabilistic versus deterministic approaches,» *Natural Hazards and Earth System Science,* vol. 20, n. 11, pp. 3135-3160, 2020.

16. A. Bozza, D. Asprone, F. Parisi e G. Manfredi, «Alternative Resilience Indices for City Ecosystems Subjected to Natural Hazards,» *Computer Aided Civil And Infrastructure Engineering,* vol. 32, n. 7, pp. 527-545, 1 June 2017.

17. G. Bellei, G. Gentile, L. Meschini e N. Papola, «A demand model with departure time choice for within-day dynamic traffic assignment,» *European Journal of Operational Research,* vol. 175, n. 3, pp. 1557-1576, 16 December 2006.

18. F. D. W. S. MD, F. T. D. V. MD, F. H. W. M. MD, R. E. A. Criss e P. Hinsberg, «Prospective validation of a new model for evaluating emergency medical services systems by in-field observation of specific time intervals in prehospital care,» *Annals of Emergency Medicine,* vol. 22, n. 4, pp. 638-645, April 1993.

19. E. B. L. M. EMT, A. J. B. M. P, J. S. MA e R. M. M. MD, «Use of a Geographic Information System to Determine Appropriate Means of Trauma Patient Transport,» *Academic Emergency Medicine,* vol. 6, n. 11, pp. 1127-1133, 2008.

20. X. M. Chen, M. L. M. Gestring, M. R. M. M. Rosengart, T. R. M. Billiar, A. B. M. Peitzman, J. L. M. M. Sperry e J. B. M. M. Brown, «Speed is not everything: Identifying patients who may benefit from helicopter transport despite faster ground transport,» *Journal of Trauma and Acute Surgery,* vol. 4, n. 84, pp. 549-557, April 2018.

21. M. E. Popescu, «LANDSLIDE CAUSAL FACTORS AND LANDSLIDE REMEDIATIAL OPTIONS,» Singapore, 2002.

22. H. F. S.-M. S. E. Kyoji Sassa, «Earthquake-Induced-Landslides: Distribution, Motion and Mechanisms,» *Soils and Foundations,* vol. 36, pp. 53-64, 1996.

23. H. R. A. S. Christofer Kristo, «Effect of variations in rainfall intensity on slope stability in Singapore,» *International Soil and Water Conservation Research,* vol. 5, n. 4, pp. 258-264, December 2017.

24. W. G. L. W. X. &. G. W. Huabin, «GIS-based landslide hazard assessment: an overview.,» *Progress in Physical Geography: Earth and Environment,* vol. 29, n. 4, pp. 548-567, 2005.

25. M. Crozier, «Deciphering the effect of climate change on landslide activity: A review,» *Geomorphology,* vol. 124, n. 3-4, pp. 260-267, December 2010.

26. F. Gabrieli, F. Gibin, L. Brezzi, E. Cernuto, A. Lupatelli, D. Salciarini, E. Mammoliti, F. Dezi, S. Stacul, N. Squeglia, A. Doglioni, V. Simeone e P. Simonini, «Lessons from international case studies on bridge-slide interaction problems,» *Procedia Structural Integrity,* vol. 64, pp. 506-513, 2024.

27. F. Guzzetti, P. Reichenbach, M. Cardinali, M. Galli e F. Ardizzone, «Probabilistic landslide hazard assessment at the basin scale,» *Geomorphology,* vol. 72, n. 1-4, pp. 272-299, 2005.

28. H. Tanyas, M. Rossi, M. ALvioli, C. J. v. Westen e I. Marchesini, «A global slope unit-based method for the near real-time prediction of earthquake-induced landslides,» *Geomorphology,* vol. 327, pp. 126-146, 15 feb 2019.

29. F. Guzzetti, S. L. Gariano, S. Peruccacci, M. T. Brunetti, I. Marchesini, M. Rossi e M. Melillo, «Geographical landslide early warning systems,» *Earth-Science Review,* vol. 200, January 2020.

30. D. Gómez, E. García e E. Aristizábal, «Spatial and temporal landslide distributions using global and open landslide databases,» *Natural Hazards,* vol. 117, pp. 25-55, 2023.

31. N. M. Newmark, «Effects of earthquakes on dams and embankments,» *Geotechnique,* vol. 15, n. 2, pp. 139-160, 1965.

32. N. Mauro, M. A. Jaimes e E. Reinoso, «Seismic-event-based methodology to obtain earthquake-induced translational landslide regional hazard maps,» *Natural hazards,* vol. 73, pp. 1697-1713, 2014.

33. e. e. h. i. t. L. A. r.-a. e.-s. p. Predicting areal limit of earthquake-induced landsliding, «Wilson, R,» *US Geological Survery Professional Paper 1360,* pp. 317-345, 1985.

34. E. Choi, R. DesRoches e B. Nielson, «Seismic fragility of typical bridges in moderate seismic zones,» *Engineering Structures,* vol. 26, n. 2, pp. 187-199, January 2004.

35. E. Erduran e A. Yakut, «Drift based damage functions for reinforced concrete columns,» *Computer and Structures,* vol. 82, n. 2-3, pp. 121-130, 2004.

36. N. I. Basöz, A. S. Kiremidjian, S. A. King e K. H. Law, «Statistical Analysis of Bridge Damage Data from the 1994 Northridge, CA, Earthquake,» *Earthquake Spectra,* vol. 15, n. 1, 1999.

37. G. a. F. L. M. Grünthal, «European Macroseismic Scale 1998,» *European Seismological Commission, Subcommission on Engineering,* 1998.

38. «IdroGEO - Torino." Accessed: Jul. 12, 2024. [Online]. Available: https://idrogeo.isprambiente.it/app/iffi/c/1272?@=45.06681018193129,7.78364491951».

39. J. W. Baker, An Introduction to Probabilistic Seismic, vol. 1.3, 2008.

40. N. Newmark, «Effects of Earthquakes on Dams and Embankments,» *Geotechnique,* vol. 15, n. 2, pp. 139-160, June 1965.

41. S. Miles e C. HO, «Rigorous landslide hazard zonation using Newmark's method and stochastic ground motion simulation,» *Soil Dynamics and Earthquake Engineering,* vol. 18, n. 4, June 1999.

42. R. W. Jibson, E. L. Harpe e J. A. Micheal, «A method for producing digital probabilistic seismic landslide hazard maps,» *Engineering Geology,* vol. 58, n. 3-4, pp. 271-289, December 2000.

43. W. J. W. Botzen, O. Deschenes e M. Sanders, «The Economic Impacts of Natural Disasters: A Review of Models and,» *Review of Environmental Economics and Policy,* vol. 13, n. 2, 2019.

44. S. K.C., «Community Vulnerability to Floods and Landslides in Nepal,» *Ecology and Society,* vol. 18, n. 1, 2013.

45. «"Banca Dati Geotecnica del Piemonte." Accessed: May. 24, 2025. [Online]. Available https://webgis.arpa.piemonte.it/agportal/apps/webappviewer/index.html?id=2067aa1af4aa44a5a6855a9d30cb5467&fbclid=IwZXh0bgNhZW0CMTAAAR3nRrbYIB9HfJuWD4_vSEtFZmb6Fzb-7QUNjVTzm».

46. 2. [. A. h.-g. "Seismic hazard model MPS04." Accessed: May. 24.

47. I. Iervolino, E. Chioccarelli e P. Cito, «Testing three seismic hazard models for Italy via multi-site observations,» 27 April 2023.

48. P. Anbazhagan, K. Bajaj, K. Matharu, S. S. R. Moustafa e N. S. N. Al-Arifi, «Probabilistic seismic hazard analysis using the logic tree approach – Patna district (India),» *Nat. Hazards Earth Syst. Science,* vol. 19, n. 10, pp. 2097-2115.

49. M. Giorgio e I. Iervolino, «On Multisite Probabilistic Seismic Hazard Analysis,» *Bulletin of the Seismological Society of America,* vol. 103, n. 3, pp. 1223-1234, June 2016.

50. «Weather Archive Pino Torinese, Accessed 1 july 2025».

51. J. T. Christian e G. B. Baecher, «D. W. Taylor and the Foundations of Modern Soil Mechanics,» *Journal of Geotechnical and Geoenvironmental Engineering,* vol. 141, n. 2, November 2014.

52. X. Z. Wu, «Development of fragility functions for slope instability analysis,» *Landslides,* vol. 12, pp. 165-175, November 2014.

53. J. Jing, Z. Wu, C. Chu, W. Ding e W. Ma, «Prediction of landslide hazards induced by potential earthquake in Litang County, Sichuan, China,» *Natural Hazards,* vol. 118, pp. 1301-1314, 2023.

54. J. Zong, C. Zhang, L. Liu e L. Liu, «Modeling Rainfall Impact on Slope Stability: Computational Insights into Displacement and Stress Dynamics,» *Water,* vol. 4, n. 16, 2024.

55. 2. [. h.-p. "Weather Archive Limone Piemonte - meteoblue." Accessed: Jul. 13.

14. APPENDICES

14.1 Appendix A

Table 10 FS and ac of Pino Nuovo road (SS10)

		m = 1		**m = 0**	
	Slope angle [°]	Factor of Safety [/]	Critical acceleration [g]	Factor of Safety [/]	Critical acceleration [g]
LPN1	8.260094926	3.14	0.31	4.53	0.51
LPN2	13.95450917	2.48	0.36	3.55	0.61
LPN3	23.62937773	1.43	0.17	1.99	0.40
LPN4	42.7284981	1.05	0.03	1.44	0.23
LPN5	26.31264849	1.29	0.13	1.78	0.35
LPN6	38.74596726	0.87	-0.08	1.17	0.11
LPN7	35.75388725	0.94	-0.03	1.28	0.16
LPN8	20.20361517	1.68	0.23	2.35	0.46
LPN9	14.49507354	2.34	0.34	3.29	0.57
LPN10	23.31770839	1.45	0.18	2.02	0.40
LPN11	13.40750844	2.53	0.36	3.56	0.59
LPN12	6.002935632	5.67	0.49	8.00	0.73
LPN13	9.501193152	3.58	0.43	5.05	0.67

Table 11 FS and ac of Pino Vecchio road.

		m = 1		**m = 0**	
	Slope angle [°]	Factor of Safety [/]	Critical acceleration [g]	Factor of Safety [/]	Critical acceleration [g]
LPV1	24.97	1.36	0.15	1.88	0.37
LPV2	10.59	3.21	0.41	4.52	0.65
LPV3	19.20	1.77	0.25	2.47	0.48
LPV4	29.35	1.15	0.07	1.59	0.29
LPV5	17.05	2.59	0.47	3.29	0.67
LPV6	25.69	1.98	0.43	2.49	0.65
LPV7	13.39	3.79	0.65	4.82	0.89
LPV8	35.18	0.81	-0.11	1.10	0.06
LPV9	27.62	1.05	0.02	1.43	0.20
LPV10	35.27	0.81	-0.11	1.10	0.06
LPV11	26.99	0.71	-0.13	1.19	0.09
LPV12	23.68	1.46	0.18	2.06	0.43
LPV13	6.00	5.67	0.49	8.00	0.73
LPV14	9.50	3.58	0.43	5.05	0.67

14.2 Appendix B

Table 12 Newmark's displacement of Pino Nuovo road (SS10)

	Slope angle [°]	Newmark's displacement [cm]	
		m=1	m=0
LPN1	8.26	0.00	0.00
LPN2	13.95	0.00	0.00
LPN3	23.63	0.00	0.00
LPN4	42.73	0.11	0.00
LPN5	26.31	0.00	0.00
LPN6	38.75	0.00	0.00
LPN7	35.75	0.00	0.00
LPN8	20.20	0.00	0.00
LPN9	14.50	0.00	0.00
LPN10	23.32	0.00	0.00
LPN11	13.41	0.00	0.00
LPN12	6.00	0.00	0.00
LPN13	9.50	0.00	0.00

Table 13 Newmark's displacement of Pino Vecchio road.

	Slope angle [°]	Newmark's displacement [cm]	
		m=1	m=0
LPV1	24.97	0.00	0.00
LPV2	10.59	0.00	0.00
LPV3	19.20	0.00	0.00
LPV4	29.35	0.00	0.00
LPV5	17.05	0.00	0.00
LPV6	25.69	0.00	0.00
LPV7	13.39	0.00	0.00
LPV8	35.18	0.00	0.00
LPV9	27.62	0.26	0.00
LPV10	35.27	0.00	0.00
LPV11	26.99	0.00	0.00
LPV12	23.68	0.00	0.00
LPV13	6.00	0.00	0.00
LPV14	9.50	0.00	0.00

14.3 Appendix C

Table 14 DS values for all the bridges included in our RN [11]

CODICE	**DESCRIZIONE**	Fragility **SLV** Moschonas (DS1)	Standard deviation	Fragility **SLV** Moschonas (DS2)	Standard deviation	Fragility **SLV** Moschonas (DS3)	Standard deviation	Fragility **SLV** Moschonas (DS4)	Standard deviation
CORSO REGINA MARGHERITA	Tre arcate in c.a. (una centrale principale e due laterali secondarie) su sei pilastri per lato	0.1	0.26828	0.28	0.2683	0.465	0.26828	0.98	0.26828
SASSI	Tre campate, di luce similare ed a unica arcata, in c.a. su due pile	0.1	0.26828	0.28	0.2683	0.465	0.26828	0.98	0.26828
V1	Cavalcavia a 9 campate con impalcati costituiti da 4 travi longitudinali,1 traverso e soletta in c.a., tipologia appoggio appoggio, c'è una frana accanto	0.1	0.26828	0.28	0.2683	0.465	0.26828	0.98	0.26828
V2	Cavalcavia a 3 campate con impalcati	0.1	0.26828	0.28	0.2683	0.465	0.26828	0.98	0.26828

	costituiti da 4 travi longitudinali,1 traverso e soletta in c.a.								
V3	Cavalcavia a 1 campata con impalcati costituiti da 4 travi longitudinali,1 traverso e soletta in c.a.	0.1	0.26828	0.28	0.2683	0.465	0.26828	0.98	0.26828
V4	Cavalcavia a 9 campate con impalcati costituiti da 4 travi longitudinali,1 traverso e soletta in c.a., tipologia appoggio appoggio, c'è una frana accanto	0.1	0.26828	0.28	0.2683	0.465	0.26828	0.98	0.26828
V5	Cavalcavia a 2 campate con impalcati costituiti da 4 travi longitudinali,1 traverso e soletta in	0.1	0.26828	0.28	0.2683	0.465	0.26828	0.98	0.26828

	c.a., tipologia appoggio appoggio								
V6	Sovrappasso lungo la SS10, in c.a.,3 campate	0.1	0.26828	0.28	0.2683	0.465	0.26828	0.98	0.26828
V7	Cavalcavia a 5 campate con impalcati costituiti da 4 travi longitudinali,1 traverso e soletta in c.a., tipologia appoggio-appoggio	0.1	0.26828	0.28	0.2683	0.465	0.26828	0.98	0.26828
V8	Cavalcavia a 3 campate con impalcati costituiti da 4 travi longitudinali,1 traverso e soletta in c.a., tipologia appoggio-appoggio	0.1	0.26828	0.28	0.2683	0.465	0.26828	0.98	0.26828
V9	Ponte ad una campata in semplice appoggio, passante sopra	0.1	0.26828	0.28	0.2683	0.465	0.26828	0.98	0.26828

	canale di deflusso acqua								
V10	Cavalcavia a 4 campate con impalcati costituiti da 4 travi longitudinali,1 traverso e soletta in c.a.	0.1	0.26828	0.28	0.2683	0.465	0.26828	0.98	0.26828
V11	Cavalcavia a 6 campate con impalcati costituiti da 4 travi longitudinali,1 traverso e soletta in c.a.	0.1	0.26828	0.28	0.2683	0.465	0.26828	0.98	0.26828
V12	Cavalcavia a 2 campate con impalcati costituiti da 4 travi longitudinali,1 traverso e soletta in c.a.	0.1	0.26828	0.28	0.2683	0.465	0.26828	0.98	0.26828
V13	Cavalcavia a 7 campate con impalcati costituiti da 4 travi longitudin	0.1	0.26828	0.28	0.2683	0.465	0.26828	0.98	0.26828

	ali,1 traverso e soletta in c.a.								

14.4 Appendix D

Figure 22 Efficiency Index for DS1

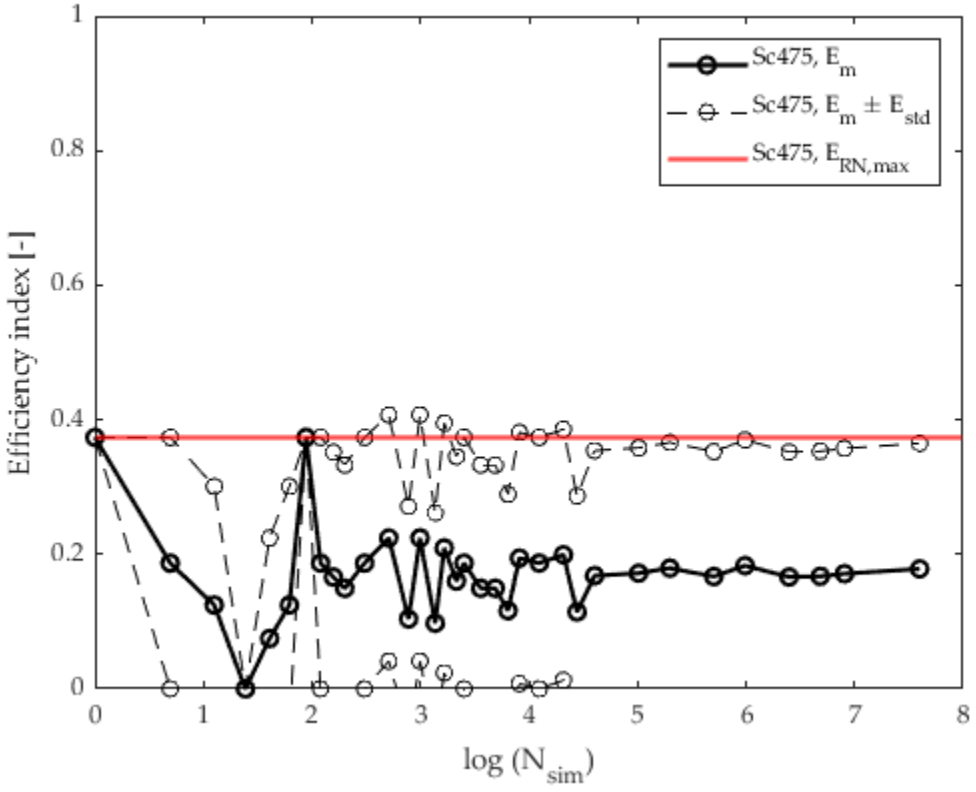

Figure 23 Efficiency Index for DS2

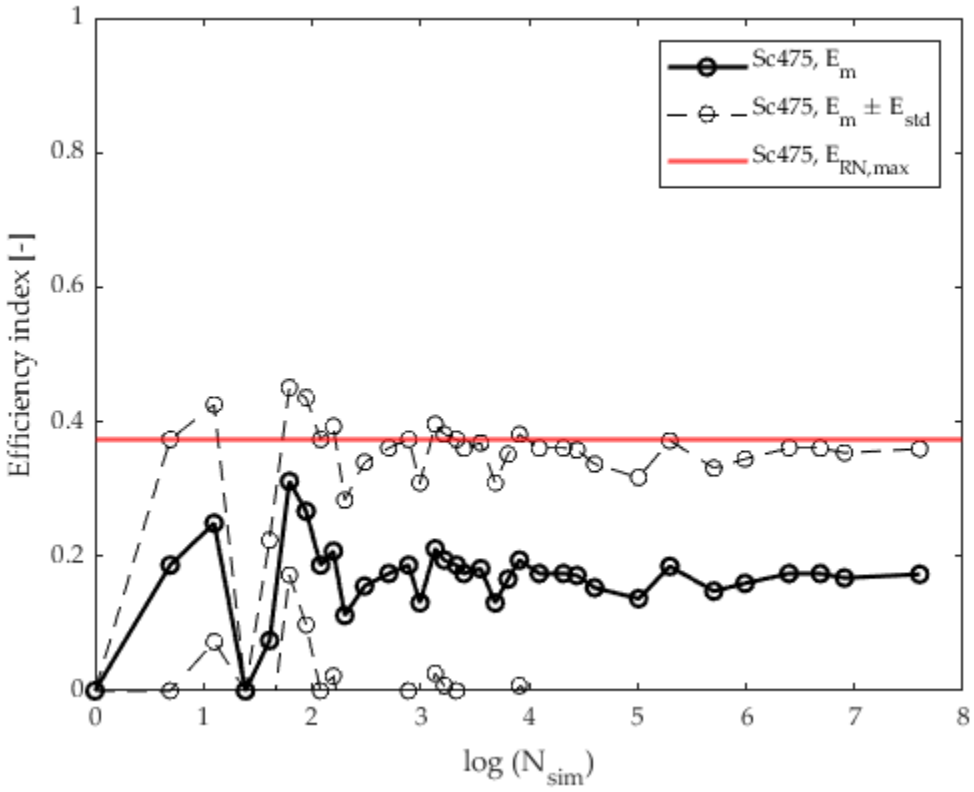

Figure 24 Efficiency Index for DS3

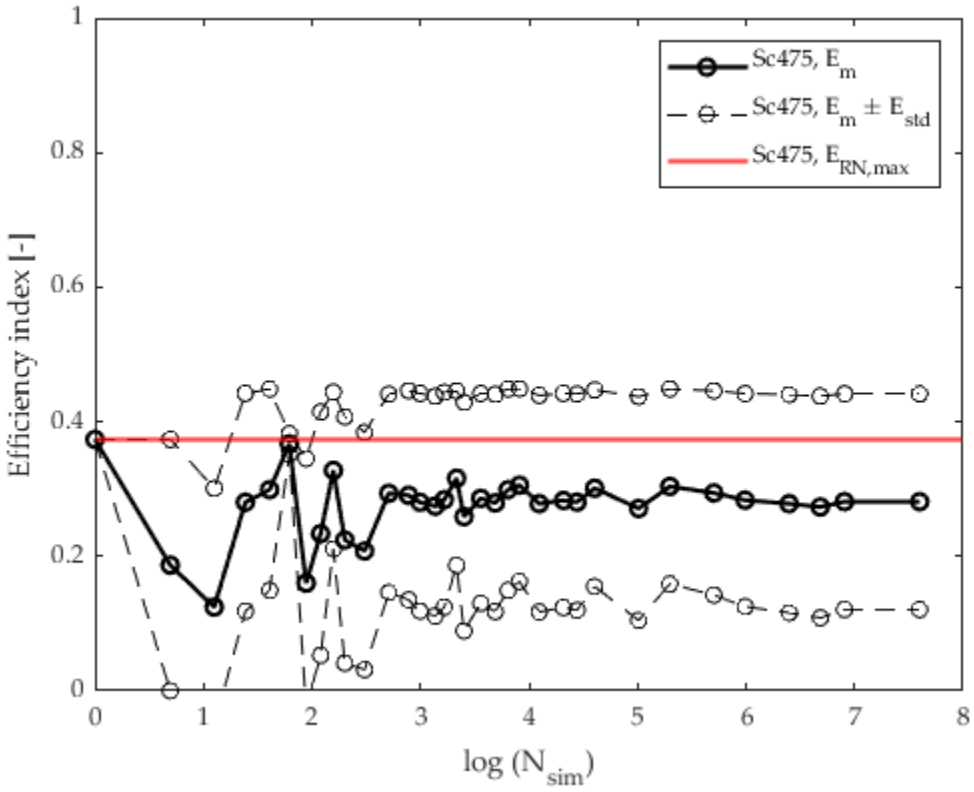

Figure 25 Efficiency Index for Ds4

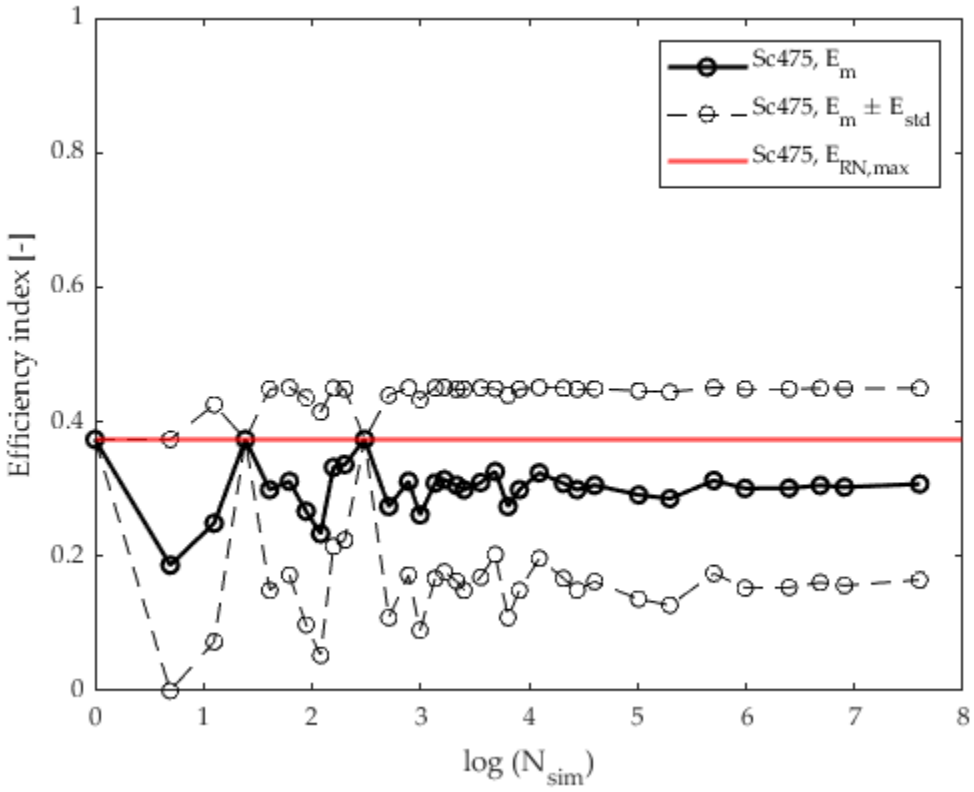

Figure 26 Efficiency Index for Ds5